CHEMICAL REVIEWS

REVIEW

pubs.acs.org/CR

Functionalized DNA Nanostructures

Ofer I. Wilner and Itamar Willner*

Institute of Chemistry, Center for Nanoscience and Nanotechnology, The Hebrew University of Jerusalem, Jerusalem 91904, Israel

CONTENTS

1. INTRODUCTION

DNA is one of the most promising materials for nanobiotechnology, and the present review article aims to describe recent advances in the self-assembly of functional DNA nanostructures. DNA exhibits nanoscale dimensions reflected by a 3.4 nm length for a complete 10-base helical turn and a diameter corresponding to 2 nm for the duplex DNA.[1] The base sequence in DNA encodes into the biopolymer tremendous structural and functional information (Figure 1). The two purine bases and the two pyrimidine bases adenine (A), guanine (G), cytosine (C), and thymine (T) constitute the building blocks of the biopolymer and provide the instructive information dictating the structure and functions of the nucleic acids. The basic Watson−Crick complementarity of A-T and C-G base-pairing leads to the formation of duplex DNA structures, and appropriate base-pairing leads to triplex-hybridization of DNA strands.[2] Also, G-rich or C-rich single-stranded nucleic acids self-assemble into G-quadruplexes[3] or i-motifs,[4] respectively, and supramolecular DNA duplexes may be cooperatively stabilized by metal ions while forming T−Hg^{2+}−T or C−Ag^{+}−C bridges.[5,6] Alternatively, the incorporation of artificial heterocyclic bases into the nucleic acid structures may provide ligation sites (ligandosides) for the bridging of duplex structures of DNA by a variety of metal ions.[7] The availability of enzymes that react with DNA/RNA, such as polymerase or reverse transcriptase, which replicate oligonucleotides, telomerase that elongates single nucleic acid strands, or sequence-specific DNA cleavage enzymes, such as endonucleases or nicking enzymes, provide a unique "toolbox" of enzymes for manipulating DNA. This arsenal of enzymes, together with the synthetic ability to synthesize any DNA sequence by automated chemical methods, and to replicate the products by the polymerase chain reaction (PCR), enable the cost-effective preparation of large amounts of any DNA. Also, ingenious organic synthesis protocols for the preparation of new nucleotide bases[8] and their biopolymers, such as peptide nucleic acids (PNAs)[9] or locked nucleotides (LNAs),[10] introduced new man-made DNA analogues revealing unique properties. These artificial DNA analogues can be conjugated to native DNA to form hybrid systems exhibiting new properties and functions.[11] Similarly, synthetic purine/pyrimidine-type bases,[12] or chemically modified nucleotides linked to redox groups,[13] photoactive units,[14] chemical functionalities (amine, thiol, azide, etc.), or molecular labels, such as biotin, provide building blocks for incorporation into the DNA chains. Such modified nucleic acids act as scaffolds for secondary chemical functionalization, for the covalent or supramolecular association of proteins, or as signal-responsive biopolymers that are activated by electrical or light stimuli.[15] Nucleic acids reveal, also, sequence-specific binding of proteins, for example, the oriC replication region in bacteria,[16a,b] the TATA box in eukaryots transcription machinery,[16c] or the aminoacyl tRNA synthetase that recognizes different tRNAs during the translation process.[16d] Also, different selection procedures, such as the systematic evolution of ligands by exponential enrichment (SELEX),[17] led to the preparation and amplification of man-made nucleic acids revealing specific binding properties toward low-molecular-weight substrates, e.g., cocaine,[18] or proteins, such as thrombin[19] or lysozyme[20] (aptamers). Also, the different selection platforms led to catalytic DNAs (DNAzymes).[21] Thus, the chemically modified DNA structures and the specific binding of proteins to DNA enable the construction of hybrid systems of predesigned structures and functions.

The control over the stabilities of duplex DNAs is achieved by the number of base-pairs, by the nature of base-pairs, and by the cooperative stabilization of the duplexes by ligand−metal bridging units. Also, external triggers, such as pH or added nucleic acid strands, may affect the duplex stabilities through the formation of single-stranded C-quadruplexes[22] or strand displacement of the duplex structures.[23] Such processes may induce topology transitions of DNA nanostructures.[24] Indeed, the control over the stabilities of DNA nanostructures by means of external triggers led to the development of DNA machines[25], such as DNA "tweezers",[26] "walker",[27] "stepper",[28] or nanometronome devices.[29] Such DNA machines were further implemented to control surface properties and functions[30] or for the development of amplified sensing platforms.[31]

Received: April 3, 2011
Published: January 10, 2012

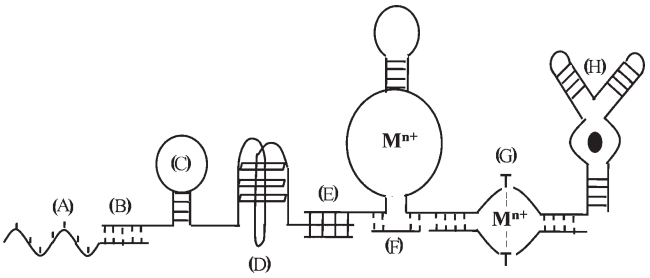

Figure 1. Schematic structural and functional features of nucleic acids: (A) single-stranded sticky end; (B) duplex hybridization; (C) hairpin nanostructure; (D) G-quadruplex; (E) triplex hybrid; (F) DNAzyme structure; (G) metal-bridged duplex; (H) aptamer nanostructure.

The self-assembly of molecular[32] or macromolecular components[33] into nanostructures is one of the most studied research topics in modern science. The continuous interest in self-assembly is inspired by the living cell machinery that demonstrates a complex system operating by self-organization principles. For example, the ribosome self-assembles by at least 3 nucleic acids and more than 50 protein units into a functional nanostructure, by implementing specific noncovalent interactions between the nucleotide bases and phosphate groups of rRNA, as well as amino acid residues of the protein subunits (H-bonds, electrostatic interactions).[34] Such self-assembly principles dictate the specific positioning of DNA, RNA, proteins, lipids, and more, in the cellular container. The resulting order controls the cell machineries, such as cell replication, ion-transport, signal transduction, metabolic enzymatic cascades and networks, fueled molecular motors, and more.

The unique features of DNA (or RNA) or of DNA/protein hybrids provide unique building blocks for the "bottom-up" assembly of nanoarchitectures that reveal programmed functionalities and properties that emerge from the one-, two-, or three-dimensional ordering of the systems. Such nanostructures can partially mimic cellular functionalities and may serve as scaffolds for the secondary templated synthesis of nanodevices. Indeed, extensive research efforts were directed in the past decade to implement the properties of DNA for the "bottom-up" self-assembly of nanostructures. Many review articles have addressed different facets of DNA nanotechnology.[35] In the present article we address the scientific advances in the self-assembly of one-, two-, and three-dimensional ordered DNA—proteins or DNA—nanoparticle nanostructures. We discuss the methods for the precise nanoscale spatial positioning of proteins or nanoparticles on the DNA scaffolds and address the emerging properties of the programmed nanostrucutres, as well as their application for the templated synthesis of nanodevices.

2. BIOCATALYTIC GROWTH OF DNA NANOSTRUCTURES THROUGH THE ROLLING CIRCLE AMPLIFICATION PROCESS

Rolling circle amplification (RCA) is a process where a circular single-stranded DNA (ssDNA) template is being replicated by DNA polymerase, with an efficient strand displacement activity, in the presence of a nucleotide mixture.[36] A short DNA strand is annealed to the circular DNA template (through base-pairing hybridization) and serves as a primer for the polymerization process. In a typical RCA process the circular template is being replicated hundreds to thousands of times, resulting in micrometers-long DNA strands of repetitive units that are complementary to the circular DNA template. These repeat units may serve as anchoring sites for different molecules, proteins, or nanoparticles (NPs). These guest substrates may be linked to the RCA product by their functionalization with nucleic acid tethers complementary to the RCA repeat units, followed by hybridization with the RCA chains. Alternatively, low-molecular-weight components, such as biotin labels, may be incorporated into the RCA products, and the biotinylated guest substrates may link to the RCA product by avidin bridges. Also, incorporation of aptamer sequences for small molecules or proteins may be used to associate these substrates into the RCA chains.

Au NPs, 5 nm, were functionalized with thiolated nucleic acids complementary to the repeat units of micrometer-long RCA products[37] (Figure 2A). Hybridization of the (**2**)-modified Au NPs to the RCA chains yielded 1D nanostructures, where the NPs were separated by equal distances (Figure 2B). The RCA process was also implemented to synthesize three-dimensional (3D) Au NPs nanostructures[38] (Figure 2C). Large Au NPs (15 nm) were functionalized with thiolated nucleic acid (**4**) (loading ca. 230 DNA strands per particle). The nucleic acid units (**4**) acted as primers that hybridized with the circular DNA template (**6**). The RCA process activated on the supramolecular structures, in the presence of polymerase and dNTPs mixture, resulted in the "decoration" of the Au NPs with long-chain RCA products in a 3D configuration. The hybridization of small Au NPs (5 nm) modified with the nucleic acid (**9**), complementary to the RCA repeat units, yielded 3D structures consisting of small Au NPs (5 nm), positioned at equal distances on the RCA chains that surround the central large Au NPs (15 nm) (Figure 2D).

Furthermore, DNA chains were generated by the RCA process using a circular DNA (**11**) and φ29 DNA polymerase in the presence of the dNTPs mixture[39] (Figure 2E). The hybridization of biotinylated nucleic acids complementary to the RCA repeat units, followed by the association of streptavidin modified with 5 nm Au nanoparticles (NPs) led to the formation of micrometer-long DNA wires on which the Au NPs-modified protein units are ordered and spatially separated by distances of 30−50 μm (Figure 2F).

Aptamers are nucleic acid sequences exhibiting specific recognition properties of low-molecular-weight substrates or macromolecules (e.g., proteins).[40] The aptamers are prepared by a selection process, systematic evolution of ligands by exponential enrichment (SELEX). The selective binding of aptamers was used to design nucleic acid chains that enabled the programmed assembly of one or two proteins on the DNA chains.[41] A circular DNA (**16**) that includes two domains that are complementary to the thrombin-binding aptamer or the lysozyme-binding aptamer was used as a template for the activation of an RCA process, in the presence of the primer, polymerase, and the dNTPs mixture. Micrometer-long RCA products (**17**) were generated, where each revolution of the RCA process generated two separated aptamer sequences against thrombin or lysozyme (Figure 3A). The selective binding of dye-labeled thrombin or dye-labeled lysozyme was monitored by AFM or confocal microscopy (Figure 3, parts B and C). For example, the thrombin units were labeled with a red fluorescent dye (tetramethylrhodamine), and lysozyme was modified with a green dye (fluorescein). The interaction of the RCA chains with the dye-labeled proteins generated the dense deposition of the two proteins (thrombin and lysozyme) on the aptamer domains (Figure 3C).

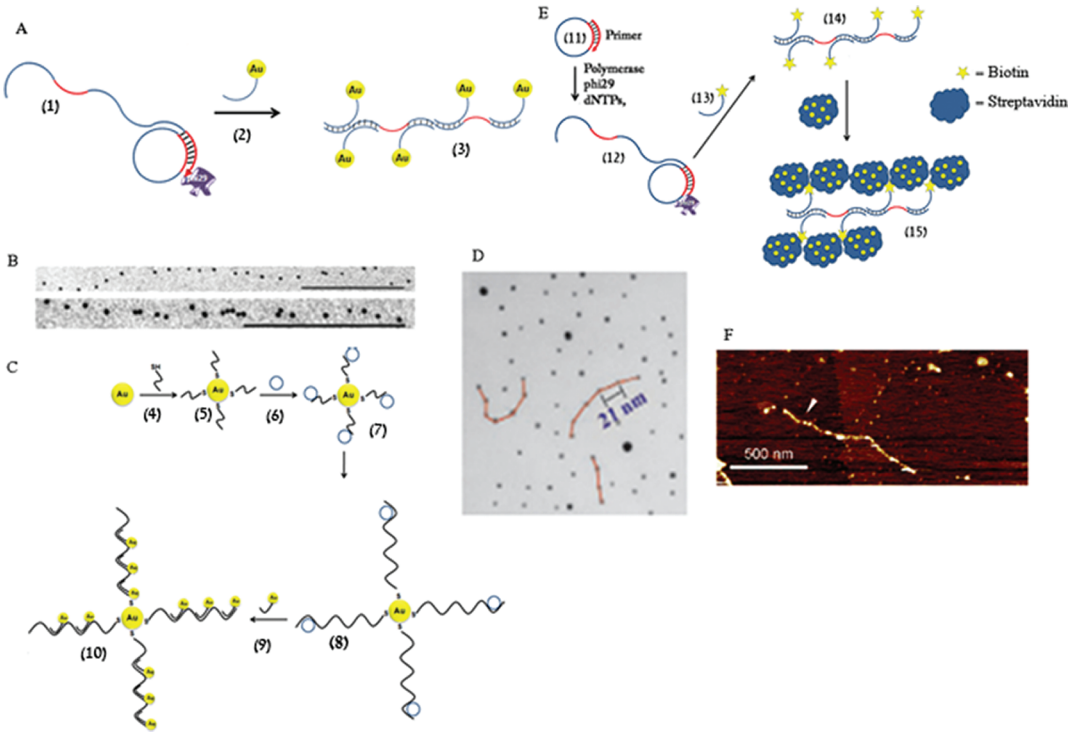

Figure 2. (A) Ordered array of Au NPs on an RCA DNA scaffold through the hybridization of nucleic acid-functionalized Au NPs on the constant repeat units of the RCA product. (B) Transmission electron microscopy (TEM) image of the ordered Au NPs array on the DNA scaffold. Reprinted with permission from ref 37. Copyright 2005 Wiley-VCH. (C) The generation of 3D Au NPs nanostructures by the primary extension of nucleic acid-functionalized Au NPs using the RCA process and by the subsequent conjugation of small Au NPs complementary to the repeat units in the RCA products. (D) TEM image corresponding to the ordered deposition of small (5 nm) Au NPs to the RCA synthesized scaffolds linked to large (15 nm) Au NPs. Reprinted with permission from ref 38. Copyright 2006 Wiley-VCH. (E) Preparation of micrometer-long DNA wires consisting of biotin-labeled nucleic acids hybridized to RCA-generated DNA scaffolds, and the assembly of Au NPs (5 nm)-functionalized streptavidin on the biotinylated DNA templates. (F) Atomic force microscopy (AFM) image of the resulting hybrid consisting of Au NPs-functionalized streptavidin on the DNA template. Reprinted with permission from ref 39. Copyright 2005 American Chemical Society.

Although the previous examples have addressed the use of the RCA products as templates for the organization of DNA/metal NPs or DNA/protein hybrid nanostructures, significant advances were achieved by demonstrating emerging functionalities of the resulting hybrid systems. For example, the RCA chains were used as templates for the activation of a bienzyme cascade[42] (Figure 3D). The circular DNA (**21**) acted as a template for the synthesis of RCA tapes consisting of constant repeat sequences I and II. The enzymes glucose oxidase (GOx) and horseradish peroxidase (HRP) were modified with nucleic acid tethers (**23** and **24**) that are complementary to the domains I and II of the RCA template, respectively. The two enzymes were then ordered on the DNA template through hybridization (Figure 3E). The spatial proximity between the two enzymes on the DNA template enabled the activation of the enzyme cascade, a process that was prohibited in the homogeneous phase. In this process, the GOx-catalyzed oxidation of glucose by O_2 yielded gluconic acid and H_2O_2, and the latter product acted as a substrate for the HRP that mediated the oxidation of 2,2′-azino-bis[3-ethylbenzthiazoline-6-sulfonic acid] ($ABTS^{2-}$) to $ABTS^{\cdot-}$. The resulting colored product, $ABTS^{\cdot-}$, provided a means to follow the enzyme cascade (Figure 3F). The programmed and ordered binding of enzymes to DNA templates for the activation of biocatalytic cascades may be extended to more complex systems. By designing circular DNAs that lead to the synthesis of DNA templates with ordered three, or more, sequence domains, the coupling of more than two enzymes may be envisaged. The hybridization of enzymes on the RCA chains enabled also the biocatalytic growth of metallic nanowires. The enzyme-mediated growth of metal nanoparticles on metal NPs seeds was extensively developed in recent years.[43,44] Specifically, the modification of enzymes, e.g., glucose oxidase (GOx), with Au NPs (1.4 nm) enabled the growth of metallic nanowires.[45] The dip-pen nanolithographic (DPN) deposition of the biocatalyst followed by the enzyme-mediated oxidation of glucose yielded H_2O_2 that acted as a reducing agent for the reduction of $AuCl_4^-$ and the enlargement of the Au NPs seeds to form Au nanowires. The advantage of the biocatalytic growth of metallic nanowires is reflected by a self-inhibition mechanism that leads to the controlled growth of the nanowires. That is, as the enzyme is coated by the enlarged NPs, the accessability of glucose to the active site is hindered, and the growth of the nanowires is blocked. These unique features of the biocatalytic growth of metallic nanoparticles and nanowires were implemented to synthesize Au nanowires on the RCA-generated template (Figure 3G). The enzyme glucose oxidase was functionalized with the nucleic acid **23**, complementary to the domain I of the RCA tape, and was further modified with Au NPs (1.4 nm). The resulting **23**/Au NPs/GOx hybrid was hybridized with the DNA template, and the biocatalytic enlargement of the NPs associated with the enzyme led to micrometer-long metal nanowires exhibiting a height of ca. 70 nm (Figure 3H).

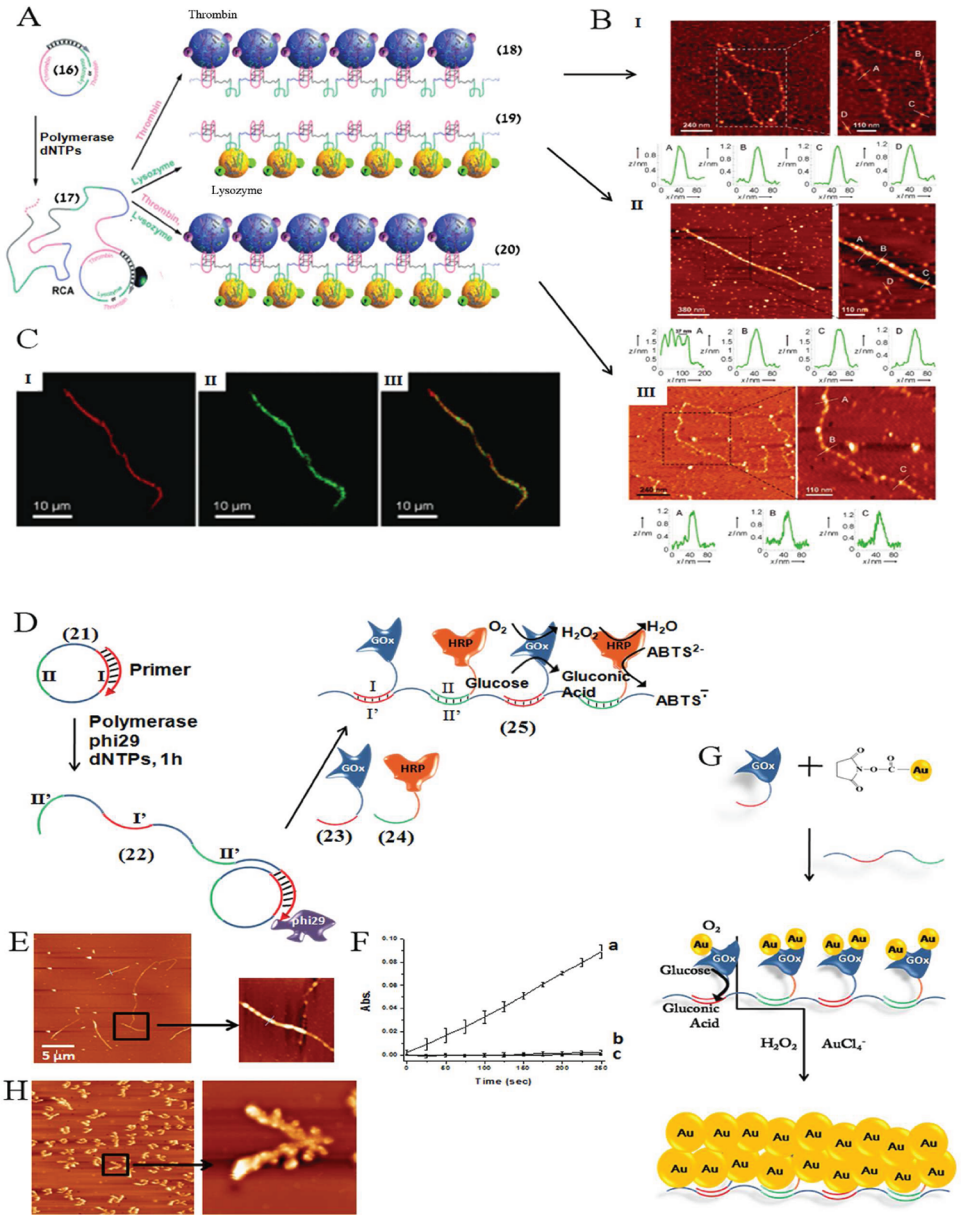

Figure 3. (A) RCA-synthesized DNA chain consisting of alternate antithrombin and antilysozyme repeat units: the selective association of TAMRA-modified thrombin and fluorescein-functionalized lysozyme on the template consisting of the two aptamers. (B) AFM images of protein−aptamer chain hybrids. (C) Confocal microscopy images corresponding to the TAMRA−thrombin and fluorescein−lysozyme proteins immobilized on the aptamer chains. (I) λ_{ex} = 543 nm, λ_{em} = 570 nm; following the TAMRA emission. (II) λ_{ex} = 488 nm, λ_{em} = 520; following the fluorescein emission. (III) Overlay of the CFM images shown in I and II. Reprinted with permission from ref 41. Copyright 2007 Wiley-VCH. (D) Synthesis of a single-stranded DNA nanowire by the rolling circle amplification (RCA) method, the programmed assembly of glucose oxidase (GOx) and horseradish peroxidase (HRP) on the DNA template, and the activation of the bienzyme cascade. (E) AFM image of the DNA nanowire functionalized with the two enzymes. (F) Kinetic data following the bienzyme cascade on the RCA-generated DNA template (a) and control experiments that monitor the bienzyme cascade in the absence of DNA or in the presence of the foreign calf-thymus DNA, (b) and (c), respectively. (G) Assembly of Au NP-functionalized glucose oxidase on the RCA-generated DNA template, and the biocatalytic growth of Au nanowires. (H) AFM image of the biocatalytically generated Au nanowire on the DNA template. Reprinted with permission from ref 42. Copyright 2009 American Chemical Society.

3. FORMATION OF FUNCTIONALIZED NANOSTRUCTURES THROUGH DIRECTED HYBRIDIZATION OF DNA TILES

DNA tiles are specific DNA constructs designed to self-assemble into one-dimensional (1D) templates,[46] two-dimensional (2D) lattices,[47] and three-dimensional (3D) nanostructures.[48] The unique features of DNA tiles include the existence of an immobile junction that rigidifies the construct and the availability of single-strand sticky-ends that allow the interhybridization of the DNA tiles and their self-assembly into complex nanostructures. Furthermore, the helical turns associated with the tiles dictate the vectorial assembly of the DNA constructs and the dimensionality of the resulting nanostructures. Figure 4 exemplifies several prototypes of reported tiles or motifs that consist of double-crossover tiles (DX),[49] triple-crossover tiles (TX),[50] 12-helix tiles,[51] 3-helix bundle tiles,[52] 6-helix bundle tiles,[53] four 4-arm junctions,[54] triangular motifs composed of 4-arm junctions,[55] cross-shaped tiles,[56] triangular DX tiles,[57]

dx.doi.org/10.1021/cr200104q |Chem. Rev. 2012, 112, 2528–2556

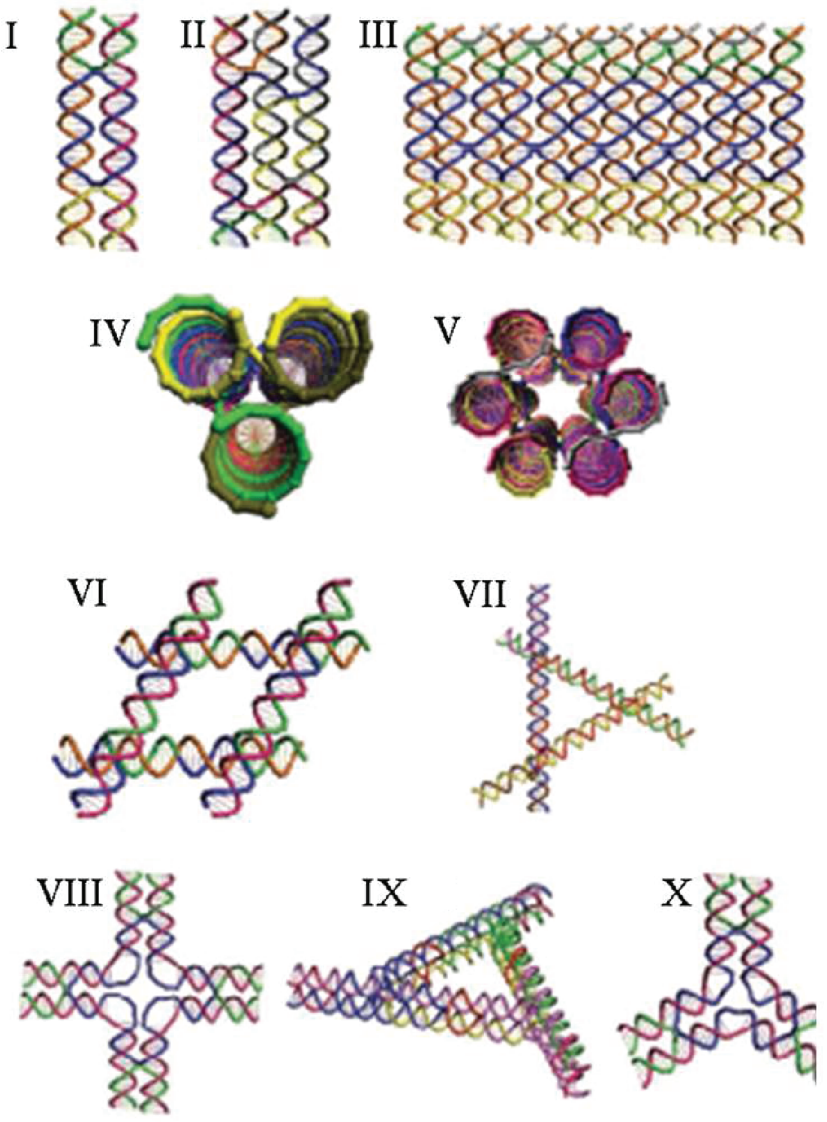

Figure 4. Examples of the toolbox of DNA tiles for the assembly of DNA nanostructures: (I) a double-crossover tile; (II) a triple crossover tile; (III) a 12-helix DNA tile; (IV) a 3-helix bundle tile; (V) a 6-helix bundle tile; (VI) a DNA tile consisting of four 4-arm junctions; (VII) a triangular motif consisting of three 4-arm junctions; (VIII) a cross-shaped tile; (IX) a triangular tile composed of three double-crossover DNA units; (X) a 3-point "star" DNA tile. Reprinted with permission from ref 35 d. Copyright 2006 Wiley-VCH.

and 3-point star DNA tiles.[58] DX consist of two helices conjugated along their long axes; TX consist of three double-stranded DNA helices lying in a plane and linked by strand exchange at four immobile crossover points; 4 × 4 tiles contain four 4-arm DNA branched junctions pointing in four directions; triangular motifs are composed of three 4-arm tiles, which are fused together; 3-helix bundle motifs contain three double helical DNA domains connected by six immobile crossover junctions. In addition to the basic property of DNA tiles to self-assemble into complex structures, one may tether to the tiles ligands on nucleic acid hinges that enable the association of NPs or proteins to the nanostructures. Alternatively, the incorporation of aptamer sequences into the tile units may provide specific binding sites for the association of proteins.

2D DNA nanocrystals were organized by the self-assembly of tiles, and these acted as scaffolds for the ordered positioning of Au NPs.[59] Four different DX tiles **a**−**d** were designed to self-assemble into 2D lattices by sticky-end cohesion (Figure 5A). Tile **b** contained a protruding sequence, modified with a thiol functionality on its 5′ end. Au NPs (1.4 nm) modified with a maleimide residue were then covalently linked to the thiol functionalities associated with the protruding units. The subsequent hybridization of the four tiles **a**−**d** resulted in the assembly of Au-nanoparticles-programmed arrays. Figure 5B outlines a TEM image of the resulting DNA crystal−Au conjugate; the interparticle spacing was found to correspond to 32 and 4 nm, respectively, as dictated by the 2D DNA scaffold.

Similarly, Au NPs were assembled on a 2D DNA scaffold, consisting of four different tiles, through base-pairing hybridization[60] (Figure 5C). Tile **f** included an extended single-stranded overhang, designed to hybridize with its complementary strand. Au NPs, 6 nm, modified with the thiolated single stranded DNA **26**, complementary to the overhanging tether of tile **f**, were subsequently incorporated into the 2D DNA scaffold, via hybridization to form an ordered Au NPs array. Topographical

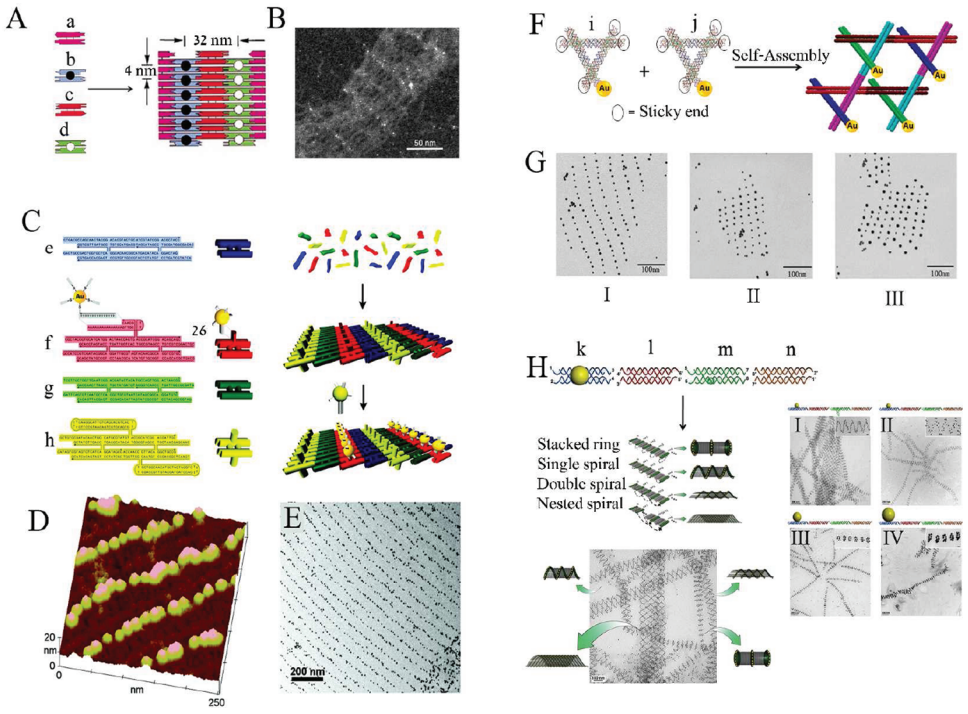

Figure 5. (A) Self-assembly of a 2D DNA nanostructure consisting of four complementary double-crossover tiles that include on tile **b** a protruding thiolated nucleic acid for the programmed immobilization of Au NPs. (B) TEM image corresponding to the spatially ordered Au NPs on the 4-tile 2D DNA array. Reprinted with permission from ref 59. Copyright 2002 Springer. (C) The self-assembly of four double-crossover tiles **e**−**h**, where tile **f** includes a protruding nucleic acid tether, and the secondary hybridization of Au NPs (6 nm) functionalized with a nucleic acid complementary to the protruding tether to yield a spatially ordered array of NPs. (D) AFM image of the resulting Au NPs array. (E) TEM image of the resulting Au NPs array. Reprinted with permission from ref 60. Copyright 2004 American Chemical Society. (F) Self-assembly of two different triangular tiles **i** and **j**, each consisting of three-dimensional double-crossover units and modified with Au NPs. (G) TEM images corresponding to (I) the 2D array formed by tiles **i** modified with 5 nm Au NPs and the bare tiles **j**. (II) The 2D array formed by tiles **i** and **j** modified with 5 nm Au NPs. (III) The 2D array formed by tiles **i** modified with 5 nm Au NPs and tiles **j** modified with 10 nm Au NPs. Reprinted with permission from ref 61. Copyright 2006 American Chemical Society. (H) Self-assembly of four different double-crossover tiles (**k**−**n**), where tile **k** includes an Au NP (of variable size) associated with a protruding thiolated nucleic acid, into nanotubes of different structures consisting of stacked ring, single spiral, double spiral, and nested spiral, and TEM images that include the different Au NPs functionalized nanostructures (I) and (II). The TEM images of the single spiral nanotubes functionalized with 5 nm Au NPs, where the structure in (I) includes on tile **m** a stem-loop component for stabilization and in (II) the nanostructure lacks this cooperative stabilization. (III) and (IV) TEM images of stacked-ring nanotubes modified with 10 and 15 nm Au NPs, respectively. Reprinted with permission from ref 62. Copyright 2009 American Association for the Advancement of Science.

AFM image of the assembled DNA array−Au hybrid, and a TEM image of the Au NPs hybridized with the DNA scaffolds are shown in Figure 5 parts D and E, respectively. The rows of the Au nanoparticles were separated by ca. 63 nm. Also, a DNA tile array for the programmed positioning of differently sized Au NPs was developed.[61] Two 3D DX triangle tiles **i** and **j** were designed to produce, upon their self-organization, a rhombic lattice arrangement (Figure 5F). Two sides of the equilateral tile contained sticky-end domains that enabled the self-organization of the nanostructure. The third side included a thiolated functionality to which Au NPs could be linked. By the mixing of the two types of tiles, 2D arrays with ordered Au NPs arrangements were prepared. Three different DNA scaffold−Au NP hybrids were constructed:

(I) By the tethering of Au NPs, 5 nm, to the thiol functionality of tile **i**, particle lines with a spatial separation of ∼54 nm in one direction and ∼27 nm in the opposite direction were generated. (II) By the tethering of the Au NPs, 5 nm, to the two tiles, NP arrays revealing closer proximity between the NPs were formed. (III) By the functionalization of tile **i** with small NPs, 5 nm, and of the thiol functionality of tile **j** with large NPs, a composite array of ordered, differently sized Au NPs was formed. The different structures were visualized under TEM; the different arrangements of the Au NPs could be obtained (Figure 5G). 3D nanostructures composed of DNA tiles, and modified with Au NPs, were fabricated.[62] Four double-crossover (DX) DNA tiles (**k**−**n**) were designed to self-assemble into a 2D array through sticky-end associations (Figure 5H). Tile **k** was modified with a thiol functionality that enabled the association of a Au NP to the tile component. While the tiles were designed to self-assemble into a two-dimensional array of Au NPs rows, due to the complementarity of the sticky-ends of the tiles, it was discovered that the tiles self-organized into tubular 3D structures consisting of tubes composed of stacked rings of Au NPs, single-spiral tubes, double-spiral tubes, and nested-spiral tubes (Figure 5H). Whereas the stacked rings were generated by the symmetrical closure of the array, the other structures were formed by nonsymmetrical folding and hybridization of the edges. The formation of the Au NP-functionalized 3D nanostructures was attributed to electrostatic repulsions among the neighboring rows of Au NPs that led to a curvature of the array, leading to its closure to the 3D nanotubes. This was supported by the fact that the self-assembly of tiles **l**, **m**, and **n** with tile **k**, lacking the Au NPs, led to the formation of only 2D arrays. Also, tile **m** was

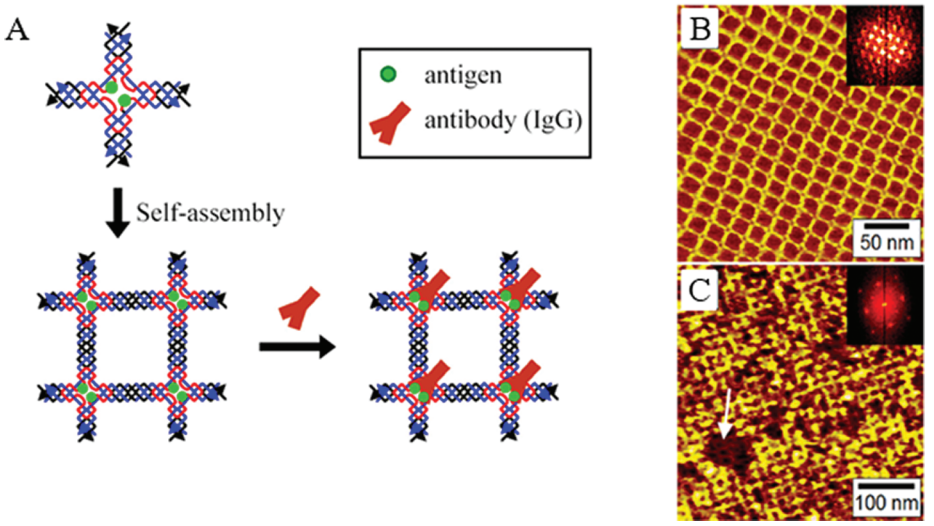

Figure 6. (A) Self-assembly of an antigen-functionalized 4-arm tile into a tetragonal square array, and the ordered binding of an antibody to the antigen sites. (B) AFM image of the antigen-modified array. (C) AFM image of the array functionalized with the antigen−antibody complexes. Reprinted with permission from ref 64. Copyright 2006 American Chemical Society.

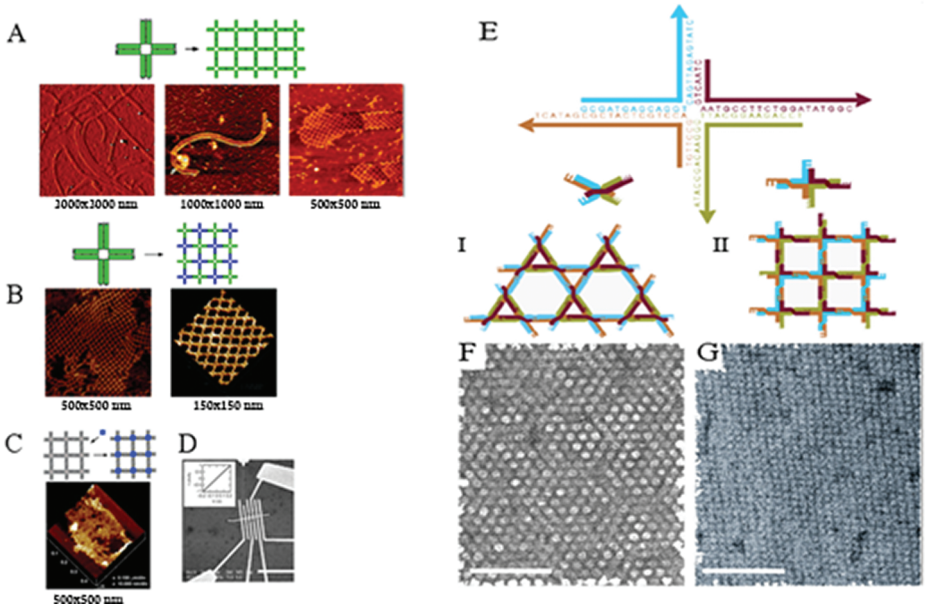

Figure 7. (A) Self-assembly of a 4-arm tile into ribbon, and 2D array nanostructures and AFM images of the resulting nanostructures: (left and middle) ribbon nanostructures and (right) two-dimensional array. (B) Self-assembly of dictated 2D arrays by the self-assembly of 4-arm tiles that constitute opposite curvatures, and AFM images of the resulting 2D arrays. (C) Self-assembly of a biotinylated four 4-arm tile into a 2D array and the association of steptavidin to the biotin sites, as well as the respective AFM image. (D) SEM image of the metalized four 4-arm nanoribbon deposited on a microelectrode array and the resulting current−voltage curve of the metallic nanowire (inset). Reprinted with permission from ref 65. Copyright 2003 American Association for the Advancement of Science. (E) Self-assembly of a Holliday-junction tile that includes two pairs of complementary sticky-ends into a Kagome lattice (I) or a square lattice (II). (F, G) TEM images of the Kagome-lattice and square-lattice nanostructures, respectively. Reprinted with permission from ref 67. Copyright 2005 Wiley-VCH.

functionalized with a stem and loop component that was designed to stabilize the two-dimensional tile structure. This nanoengineering effort turned out to be unsuccessful, and the electrostatic repulsions between the Au NPs rows predominated to yield the 3D tubes. It was found, however, that the removal of the stabilizing stem and loop components resulted in nanotubes of smaller diameter, consistent with the enhanced electrostatic-driven closure of the edges. Figure 5H (I−IV) outlines TEM images that represent the four different tubular structures that were formed.

In nature, the spatial organization of proteins and cofactors is an essential feature for stimulating biocatalytic processes, such as the photosynthesis, the mitochondrial respiratory chain, and the signal-transduction reactions. Thus, artificial systems designed to spatially order programmed structures of proteins are taking a leading role in the field of synthetic biology.[63] The unique properties of DNA nanostructures generated by the 2D and 3D assembly of tile elements turn them into natural candidates for scaffolding and organizing proteins and cofactors.

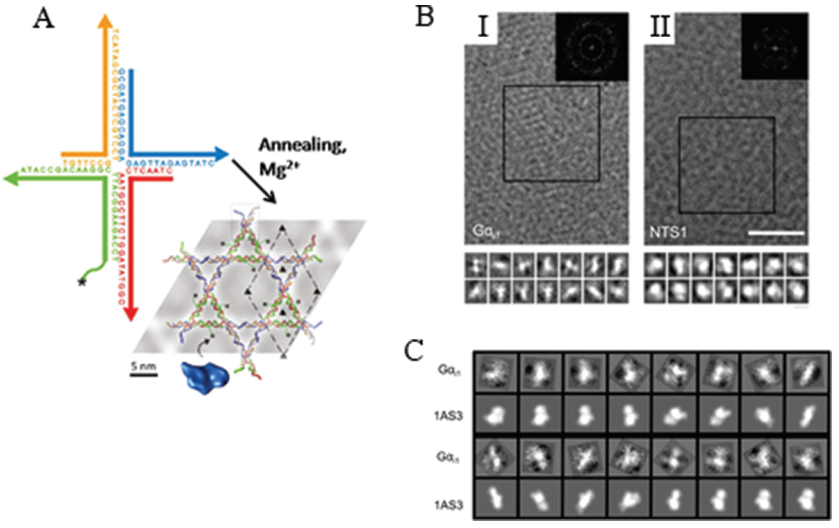

Figure 8. (A) Self-assembly of a 4-arm Holliday-junction tile functionalized with either NTA or neurotensin peptide (NT) ligands into the Kagome-type lattices. (B) Cryo-TEM images of the $G\alpha_{i1}$ (I) or of the neurotensin receptor type 1(NTS1) (II), linked to the respective ligand-functionalized Kagome-type lattices. (C) Single-molecule projections of the $G\alpha_{i1}$ linked to the NTA-functionalized Kagome-type lattice in comparison to the projection of the crystal structure of the protein available PDB: 1AS3. Reprinted with permission from ref 68a. Copyright 2011 American Chemical Society.

The self-assembly of 4-arm tiles into tetragonal square arrays through sticky-ends hybridization was used for the ordered positioning of antibodies on the array[64] (Figure 6). The cross-over DNA tiles included in their center the fluorescein antigen. After the polymerization of the tiles to the array (Figure 6A), the antifluorescein antibody was associated with the antigen units. The AFM images (Figure 6, parts B and C) revealed heights of 1.7−1.9 nm for the DNA arrays and 2.7−3.5 nm for the antibody modified arrays.

Other self-assembled DNA nanostructures composed of nucleic acid tiles acted as scaffolds for the ordered organization of proteins. For example, a DNA tile composed of 4 arms with opposite sticky-end complementarities was used as a subunit to assemble the nanostructure[65] (Figure 7A). The resulting nanostructures consisted mostly of ribbon-like tubular objects that originated from an intrinsic curvature in the tile, leading to the folding of the array into the tube configuration and to a low population of unfolded 2D tile arrays. AFM measurements of the resulting array showed a center-to-center distance of 19 nm. By the further design of 4-arm tiles exhibiting opposite curvatures and appropriate sticky-end complementarities, unfolded two-dimensional arrays were formed (Figure 7B). By the incorporation of biotin labels into the center of the tiles, the dictated binding of streptavidin to these sites was accomplished (Figure 7C). The streptavidin-modified array revealed a height of ca. 5 nm. Furthermore, the ribbon-like tubular structures, generated by the self-assembly of a single tile with intrinsic curvature, acted as a scaffold for the synthesis of metallic nanowires. The metallization of Ag^+- functionalized ribbons and their deposition on a microelectrode array (Figure 7D) demonstrated the formation of conductive metallic nanowires. (For further DNA devices, see section 6). A protein linked to the DNA components may also dictate the structural features of the DNA nanostructure. This was exemplified with the use of the RuvA bacterial recombination protein that included the formation of a two-dimensional DNA structure that differs from the DNA nanostructure formed in the absence of RuvA. RuvA is part of the "resolvasome" protein complex that includes also RuvB and RuvC. It protects Holliday junctions from unwinding while promoting branch migration.[66] This property of RuvA was used to bind and position the protein to artificial Holliday junctions comprising of DNA tiles.[67] DNA tiles consisting of 4 arms of an immobile Holliday junction that include sticky-ends were used to self-assemble the nanostructures (Figure 7E). As two configurations of the Holliday junction are possible, their polymerization into different nanostructures is feasible: (I) Polymerization of the *x*-stacked junction, which yields a Kagome lattice and (II) the assembly of the square-planar junction, which self-assembles into a square lattice (Figure 7E). The RuvA protein binds to the center of the Holliday junction and rigidifies the tile into the square-planar junction that leads to the self-assembly of the square-lattice system. In contrast, in the absence of RuvA the formation of the Kagome lattice is energetically favored. The TEM images of the resulting Kagome lattice, in the absence of RuvA, and the RuvA-induced square-lattice nanostructures are depicted in parts F and G of Figure 7, respectively.

In a related study, a Kagome lattice of DNA was used as a template for the organization of proteins on the array, and the use of the nanostructures for single-molecule imaging of proteins was demonstrated.[68a] A four-component oligonucleotides Holliday junction tile, which includes 4 double-stranded arms with sticky-ends, was used to self-assemble the Kagome-type trigonal 2D crystalline DNA array (Figure 8A). One of the oligonucleotides was labeled with either the trisnitrilotriacetic functional group (tri-NTA)[68b] or with the neurotensin peptide (NT). The NTA-modified array was used to selectively bind the His-6 functionalized guanine nucleotide-binding protein (Ga_{i1}) to the NTA sites through the formation of the respective NTA-Ni^{2+}-His-tag complex. Similarly, the neurotensin receptor type 1 (NTS 1) was bound to the NT sites associated with the 2D crystalline lattice. The concentration of the proteins on the DNA template enabled the cryo-TEM imaging of a single protein on the surface (Figure 8B). The imaged projections of the Ga_{i1} protein

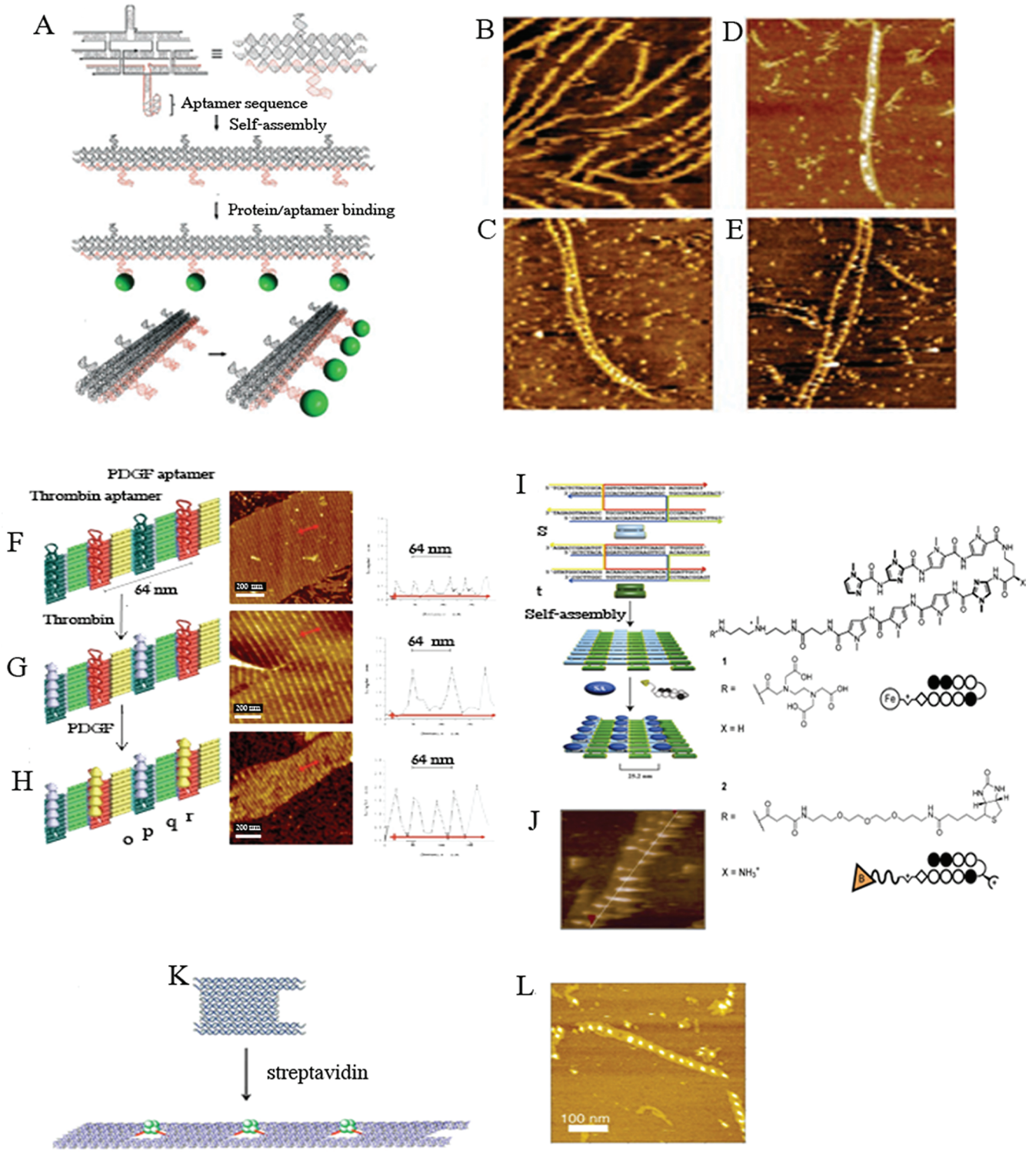

Figure 9. (A) Self-assembly of a triple-crossover tile with sticky-ends that includes a protruding antithrombin aptamer sequence and the association of thrombin to the resulting nanostructure. (B) AFM image of the resulting structure prior to the binding of thrombin. (C−E) AFM images of the thrombin-modified nanostructures. Reprinted with permission from ref 69. Copyright 2005 Wiley-VCH. (F) Self-assembly of four DX tiles (**o**−**r**) that include protruding aptamer sequences against thrombin DX (**p**) and against PDGF DX (**r**), as well as the respective AFM image and cross-section analysis. (G) After immobilization of thrombin to the aptamer sites. AFM image and respective cross-section analysis are shown. (H) After coassociation of PDGF to the thrombin-modified nanostructure. AFM image and cross-section analysis are shown. Reprinted with permission from ref 71. Copyright 2007 American Chemical Society. (I) Self-assembly of two DX tiles **s** and **t** that include sticky-ends and a specific sequence that binds biotinylated polyamide. Streptavidin was linked to the biotin sites on the resulting nanostructure. (J) AFM image of the spatially ordered streptavidin units on the DNA array. Reprinted with permission from ref 73. Copyright 2007 Wiley-VCH. (K) A "U"-shaped tile with sticky-ends that self-assembles into a strip that includes biotin-labeled DNA-free wells. Streptavidin binds to the biotin sites to yield the spatially ordered protein−DNA nanostructure. (L) AFM image of the resulting nanostructure. Reprinted with permission from ref 75. Copyright 2008 Wiley-VCH.

dx.doi.org/10.1021/cr200104q |*Chem. Rev.* 2012, 112, 2528–2556

correlated well with the projection of the high-resolution crystal structure of this protein (Figure 8C).

Aptamer sequences were used to link a protein to ordered nanoengineered sites on a self-assembled 1D DNA nanostructure.[69] A triple-crossover (TX) DNA tile was used to construct a one-dimensional array (Figure 9A). The TX tile had two protruding DNA loops, where one included the 15-base thrombin binding aptamer sequence and the other served as a control sequence. The TX tile self-assembled into a 1D nanostructure that included the thrombin-binding-aptamer units, at a periodic distance of ~17 nm (Figure 9B). Addition of thrombin to the solution resulted in a periodic linear array of thrombin molecules. Thrombin associated with the aptamer sites and resulted in the programmed positioning of the protein on the 1D ribbon (Figure 9C–E). AFM analyses reveal a height of 1.7 nm for the DNA arrays and 2.5–3 nm for the thrombin-modified DNA arrays. The lateral distance between adjacent protein molecules was 17–19 nm. Interestingly, many of the resulting ribbons revealed double-chain nanostructures that indicated interchain interactions. These were attributed to the dimerization of thrombin units that bind to aptamer sites on adjacent chains.[70] Similarly, two different proteins were patterned onto a periodic 2D DNA nanoarray using two different aptamers, one for each protein.[71] A set of four double-crossover (DX) tiles was used to self-assemble the DNA nanostructure (Figure 9F). Tile **p** included a protruding thrombin-binding aptamer sequence, whereas tile **r** was functionalized with the aptamer sequence against the platelet derived growth factor (PDGF). Figure 9(F–H) outlines the AFM images corresponding to the stepwise assembly of the DNA array and the subsequent binding of the two proteins on the DNA template. The array of the tiles (Figure 9F) consists of parallel lines of the alternate protruding aptamer sequences separated by a distance of 32 nm (revealing a height of ca. 0.7 nm). Interaction of the DNA array with thrombin led to the specific binding of the protein to the thrombin-binding aptamer sequences separated by distances corresponding to ca. 64 nm (revealing a height of ca. 2 nm) (Figure 9G). The subsequent binding of PDGF to the free anti-PDGF domains results in the densely organized nanostructure where the two proteins were spatially separated one from another by a distance of 32 nm (Figure 9H). A related approach was implemented for the optical detection of thrombin on a two-dimensional DNA array.[72] A set of two DX tiles, where one of the tiles included a protruding nucleic acid tether consisting of the thrombin-binding aptamer sequence that was labeled with the 3-methylisoxanthopterrin dye, was used. In the presence of thrombin, the aptamer sequence folded into a G-quadruplex, while forming the aptamer–thrombin complex. The fluorescence of the labeling dye is enhanced in the resulting G-quadruplex, a property that was used to follow by confocal microscopy the binding of thrombin to the array. Further studies have applied the highly specific biotin–streptavidin affinity interactions to assemble the protein on an array of DNA tiles.[73] Two DX tile elements, **s** and **t**, were used to generate a two-dimensional array of the tiles, through sticky-end hybridization. The tile **s** included the specific sequence that binds the biotin-labeled pyrrole–imidazole polyamide ligand (Figure 9I). The subsequent association of streptavidin yielded an organized nanostructure where the protein units are periodically assembled on the respective tile units. Figure 9J shows an AFM image of the resulting DNA–thrombin hybrid array. The average spacing between individual streptavidin molecules was found to be ca. 24 nm, consistent with the expected dimensions of the 2D array. This concept was further extended to program the positioning of proteins on a single DNA nanostructure.[74] An array consisting of four different double-crossover (DX) tiles with appropriate sticky-ends was used to assemble the 2D array. The base sequence encoded in the tiles provided the program for the specific association of three different biotinylated polyamides in sequence-directed, spatially separated domains on the array. The subsequent binding of streptavidin to the biotin units led to the generation of six different patterns of predesigned separation between the proteins. A parallel study demonstrated the assembly of two-dimensional tapes of DNA that included periodically ordered pores, and the spatial programmed assembly of tetrameric streptavidin into the pores was achieved[75] (Figure 9K). A "U"-shaped DNA structure was designed to self-assemble, through sticky-end hybridization, into a two-dimensional tape that included periodically ordered pores. The substitution of the pore sites with biotin labels resulted in the selective binding of tetrameric streptavidin to the pores (Figure 9L). The average hole-to-hole distance was found to be ca. 26 nm, and the streptavidin-modified array revealed heights of ca. 3 nm.

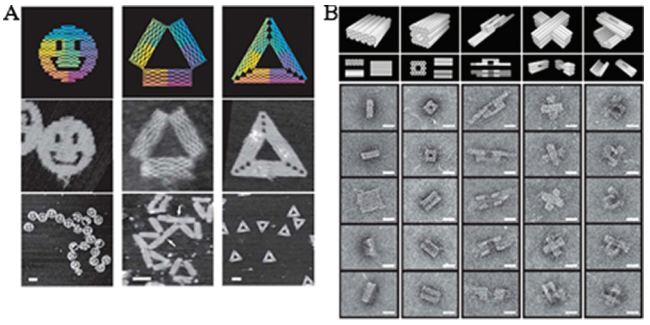

Figure 10. (A) AFM images of two-dimensional origami nanostructures. Reprinted with permission from ref 76. Copyright 2006 Nature Publishing Group. (B) Cryo-TEM images of three-dimensional DNA origami nanostructures. Reprinted with permission from ref 77c. Copyright 2009 Nature Publishing Group.

4. FUNCTIONAL DNA NANOSTRUCTURES THROUGH DIRECTED ORIGAMI FOLDING

DNA origami-based nanostructures are generated by the folding of a viral DNA strand into two-dimensional or three-dimensional nanostructures using short complementary nucleic acid sequences acting as "staple" units for the viral DNA. By the appropriate design of the staple units, nanostructures of precise geometries exhibiting nanometer-scale resolutions may be assembled. This paradigm was pioneered by Rothemund[76] with the seminal demonstrations that appropriate selection of staple units may lead to predesigned nanoscale 2D or 3D[77] shapes and patterns of DNA (Figure 10). One of the challenges in the self-assembly of DNA-origami-based nanostructures involves the appropriate design of the staple strands. To date, computer softwares are available[78] to design the appropriate staple units. Not surprisingly, the design of programmed origami-based DNA assemblies provided the basis to organize ordered systems of nanoparticles, nanotubes, and proteins on origami scaffolds.

DNA origami nanostructures were used as templates for the precise positioning of Au NPs.[79] Lipoic acid-modified Au NPs that included a bivalent thiolate–Au linkage were prepared, and

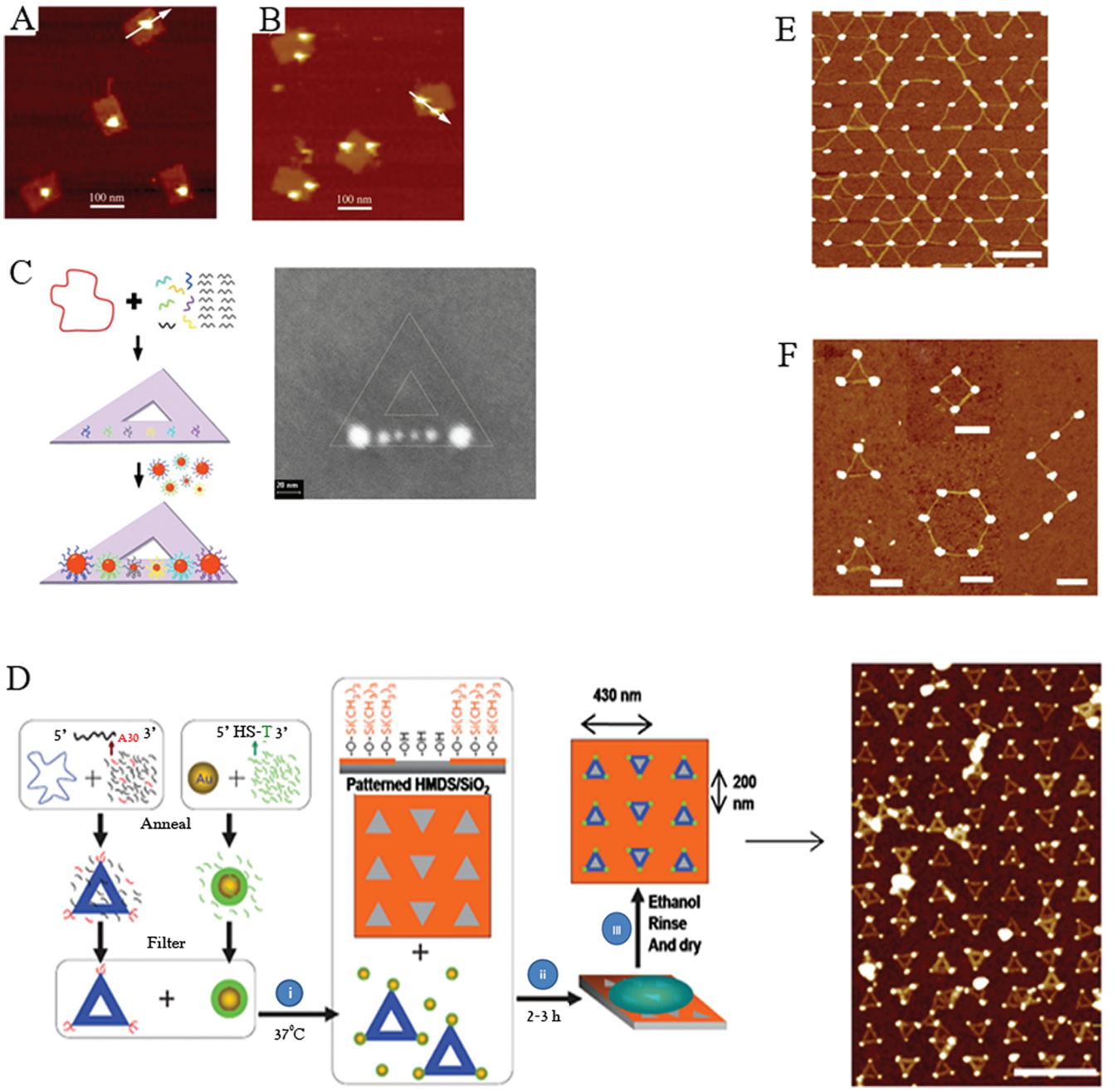

Figure 11. Programmed positioning of Au NPs (10 mm) onto rectangular origami nanostructures by the incorporation of Au NPs-functionalized staples into the set of origami staples. (A) AFM image of the nanostructure generated using a single Au NP-functionalized staple. (B) AFM image of the nanostructures obtained by the use of two different Au NP-functionalized staples. Reprinted with permission from ref 79. Copyright 2008 American Chemical Society. (C) Self-assembly of an origami triangular nanostructure that includes protruding nucleic acid tethers for the specific addressing of Au NPs of variable sizes through hybridization. Right: SEM image of the resulting ordered Au NP array. Reprinted with permission from ref 80. Copyright 2010 American Chemical Society. (D) Self-assembly of triangular origami nanostructures modified at their corners with Au NPs (5 nm) through hybridization to protruding tethers. Triangles were self-assembled on a silicon wafer that was photochemically patterned with hydrophilic/hydrophobic domains; Au NP-modified triangles were selectively associated to the hydrophilic regions. Right: the resulting AFM image. Reprinted with permission from ref 81b. Copyright 2010 Nature Publishing Group. (E and F) AFM images of photolithographically generated Au patches on a silicon wafer and the addressed positioning of thiolated origami nanotubes in between the Au patches. Reprinted with permission from ref 82. Copyright 2010 American Chemical Society.

their assembly to the origami nanostructure was compared to the assembly of monothiolated Au NPs. The viral DNA was folded using ca. 200 appropriate staple nucleic acids that order the origami DNA into a rectangular template. By the incorporation of a single 10 nm Au NP functionalized with one of the staple elements, or two types of 10 nm Au NPs functionalized with two different staple units in the self-assembly mixture, rectangular DNA nanostructures were generated with the selective binding

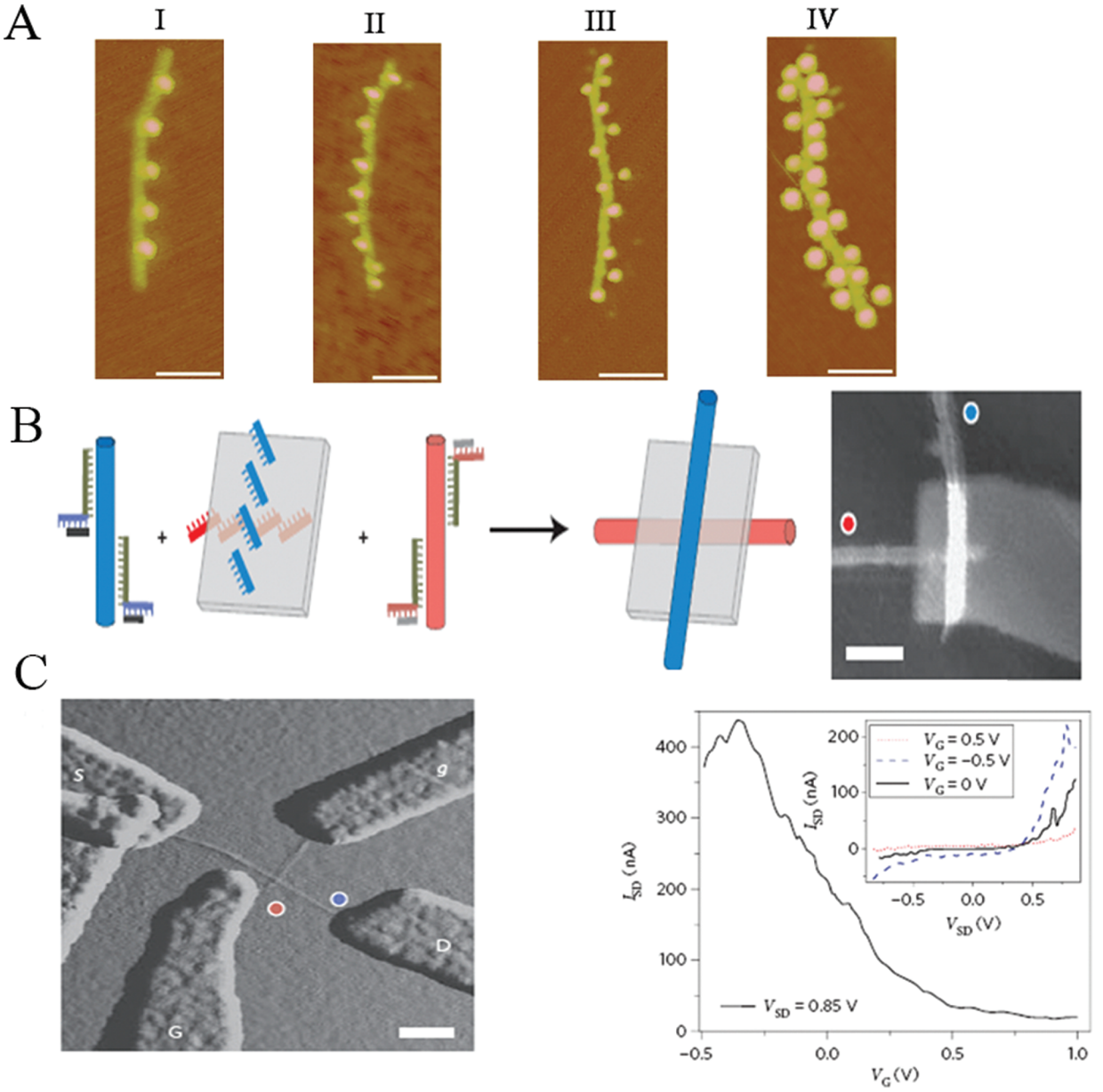

Figure 12. (A) AFM images of origami-folded six-helix DNA tubules that include protruding biotinylated tethers at programmed spatial distances on the tubules. CdSe/ZnS quantum dots (15−20 nm) were functionalized with streptavidin and linked to the spatially separated tethers: (I) 71 nm, (II) 43 nm, (III) 29 nm, and (IV) 14 nm. Reprinted with permission from ref 85. Copyright 2010 American Chemical Society. (B) Rectangular origami structure that include protruding tethers above and below the origami plane. Carbon nanotubes (CNTs) were wrapped with nucleic acids that included sticky-ends with specific complementarity to the tethers above and below the origami plane. This resulted in the orthogonal deposition of the CNTs on the respective domains. Right: AFM height image of the CNTs of the resulting origami/CNTs hybrid. (C) Deposition of the origami−CNTs nanostructure on a four-microelectrode pattern. Left: AFM amplitude image. Right: Current−voltage curve of the resulting device demonstrating transistor behavior. Reprinted with permission from ref 86. Copyright 2010 Nature Publishing Group.

of one (Figure 11A) or two Au NPs (Figure 11B), respectively. AFM images revealed a spacing of ~47 nm between two adjacent Au NPs, and a height of 12 nm, consistent with the expected height of a 10 nm Au NP over a double-stranded DNA scaffold. It was also found that the yield of binding of the Au NPs to the origami scaffold was significantly improved upon binding of the lipoic acid-modified NPs as compared to the monothiolate NPs (91% vs 45%). In a related study,[80] a triangular DNA origami scaffold was prepared, and three Au NPs of variable sizes (15, 10, and 5 nm), each modified with a nucleic acid complementary to a protruding target sequence, were directed and ordered on the origami nanostructures (Figure 11C). A center-to-center distance of 90 nm between two 15 nm Au NPs was measured, consistent with the design. DNA/origami hybrid structures were further organized in microscale assemblies on surfaces.[81] DNA origami triangles were assembled by using the appropriate mixtures of staple nucleic acids that linked together the M13 phage DNA to the triangle template. Au NPs (5 nm) were modified with a nucleic acid complementary to protruding sequences associated with the staples at the corners of the triangles. The interaction of the functionalized Au NPs with the origami-based template led to the positioning of the Au NPs

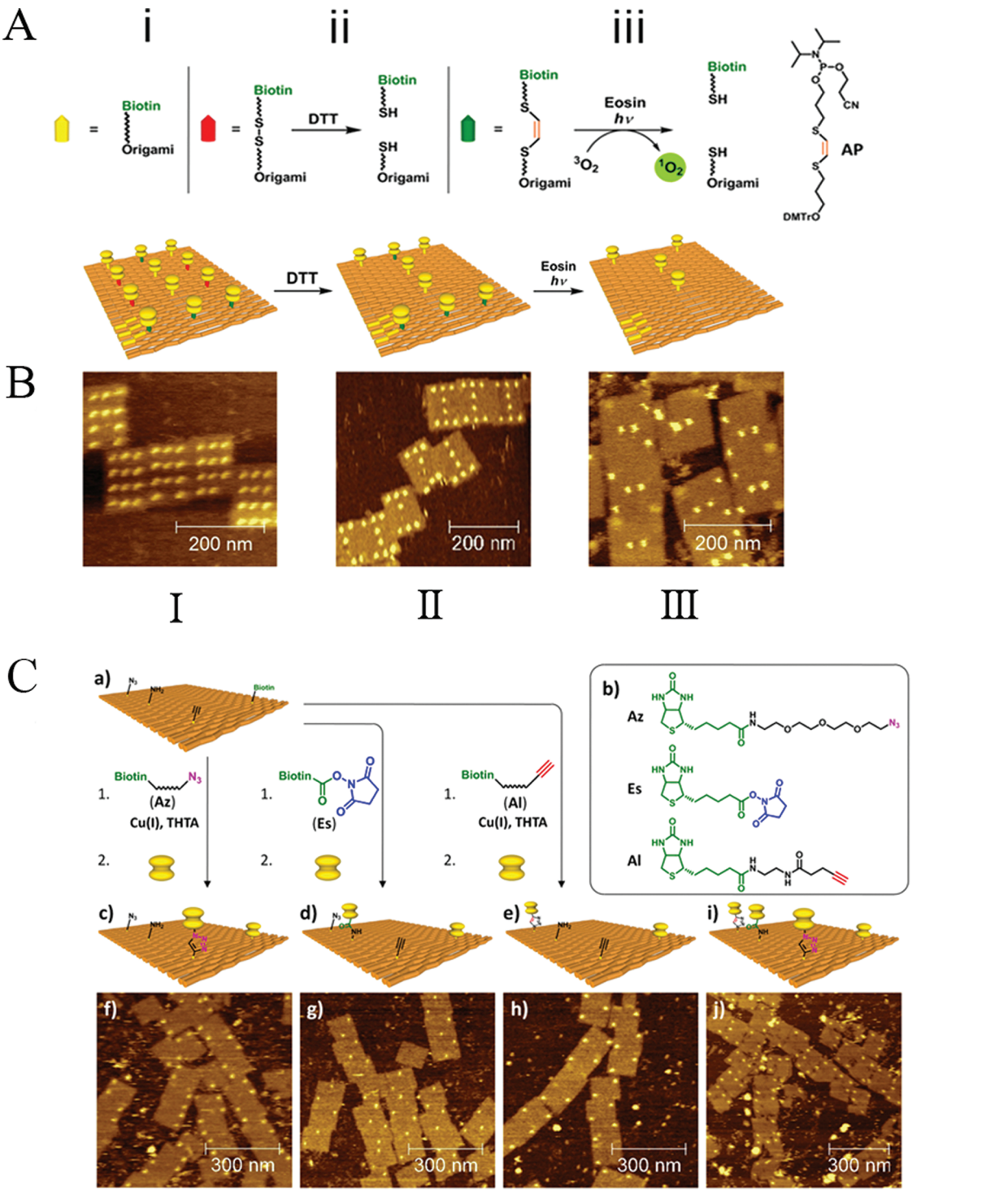

Figure 13. (A) Stepwise chemical manipulation of an ordered streptavidin−origami DNA hybrid nanostructure. Twelve biotinylated staple units were included in the set of DNA staples to organize a rectangular origami DNA to yield a programmed order of the biotin units on the nanostructure. The 12 biotinylated staples include three classes of biotin-labeled nucleic acid: (i) noncleavable, (ii) disulfide-bridged-cleavable by thiols, and (iii) ethylene-bridged nucleic acid photochemicaly cleaved by $^1O_2$. Streptavidin was attached to all biotin sites and sequentially removed from the nanostructure by the respective chemical transformation. (B) AFM images corresponding to (I) streptavidin bound to all biotin sites; (II) after removal of the streptavidin linked to the disulfide bridged biotins; (III) after photochemical removal of the ethylene-bridged biotins with $^1O_2$. (C) (a) to (e) Spatial functionalization of an origami DNA nanostructure for specific attachment of proteins. Three different biotin labels modified with an azide, *N*-hydroxysuccinimide (NHS, active ester), or alkyne were covalently coupled to spatially separated protruding staple units modified with alkyne, amino, and azide functionalities, respectively. By the stepwise chemical functionalization of the origami array with the biotin units, spatial addressing of streptavidin was achieved. Bottom: AFM images corresponding to the association of streptavidin: (f) the biotin linked to the alkyne sites; (g) the biotin bound to the amine sites; (h) the biotin linked to the azide sites; and (j) streptavidin linked to all three types of biotin sites. Reprinted with permission from ref 87b. Copyright 2010 Nature Publishing Group.

dx.doi.org/10.1021/cr200104q |*Chem. Rev.* 2012, 112, 2528–2556

at the corners of the triangle. A silicon surface was lithographically patterned by e-beam lithography, leading to hydrophilic patterned domains separated by hydrophobic regions. The interaction of the presynthesized DNA origami−Au NP structures with the surface led to the binding of the hydrophilic origami nanostructures on the hydrophilic patterns; the DNA Au NPs pattern dimensions corresponded to 430 nm between columns of triangles and 200 nm between rows (Figure 11D). In a related work, surfaces were lithographically patterned with Au patches, and folded origami nanotubes with lengths corresponding to 380 nm, which included protruding thiol functionalized nucleic acids, were positioned in between the Au domains.[82] Figure 11E depicts the AFM image of the origami DNA nanotubes deposited on a hexagonal lattice of patterned Au domains. Similarly, Figure 11F reveals the AFM image of origami DNA tubes positioned on different patterns of Au domains. These studies demonstrate the integration of DNA nanotubes on top-down lithographically patterned circuits. In related studies, other origami nanostructures were deposited on a lithographically patterned surface,[83] and origami nanostructures functionalized with Au NPs were integrated with Au patterns.[84]

The DNA origami method was also implemented to assemble CdSe/ZnS quantum dots (QDs), 15−20 nm, with programmed spacing.[85] The M13 phage DNA was folded into six-helix DNA tubules using ca. 200 staple sequences. Biotinylated staple units were placed at programmed spatial distances, and streptavidin-labeled QDs were linked to the biotin tethers. Using periodic separation distances of the biotin labels that consisted of 71, 43, 29, and 14 nm, the QDs were positioned at programmed distances on the DNA tubules (Figure 12A). It was found that, although the positioning of the QDs at large separation distances (71, 43 nm) followed the original design, at shorter distances between the QDs, the ordering was found to be perturbed, presumably due to electrostatic repulsion between the QDs.

Carbon nanotubes (CNTs) find growing interest as functional units in nanoscale electronic devices. The DNA origami scaffold was used to organize ordered carbon nanotubes in a predesigned configuration[86] (Figure 12B). The M13 phage DNA was interacted with a nucleic acid mixture, acting as staples, to form a 2D rectangular DNA structure. A set of the staple units were designed to include a protruding nucleic acid chain that was positioned vertically above the 2D origami array, whereas a second set of staple units included the protruding nucleic acid chains in a horizontal configuration, below the origami array. By the modification of carbon nanotubes with nucleic acids complementary to the respective protruding tethers, the carbon nanotubes were positioned on the vertical/horizontal domains. Figure 12C shows an AFM image of two SWNT aligned perpendicularly, on the origami template. The CNTs assembled on the DNA origami template were then deposited on a silicon substrate, modified with four Pd/Au microcontacting electrodes. The resulting nanostructure revealed field effect transistor (FET) characteristics (Figure 12C). (For further applications of DNA nanostructures to assemble nanoscale devices, see vide infra).

The origami scaffold was further used for the distance-dependent multivalent ligand−protein binding[87a] and for driving specific reactions with precise positioning of proteins at the single molecule level.[87b] The M13 phage DNA was organized into a rectangular DNA origami pattern using a set of ∼200 staple strands that included 12 biotinylated staples. The biotinylated staples included three types of staple units: four of the staples included noncleavable biotin units, four other staples included a disulfide bridge to a nonstapling biotinylated nucleic acid, and a third class of four staple nucleic acids was linked by an ethylene, electron-rich bridge to a nonstapling biotinylated nucleic acid. The stapled origami nanostructure resulted in the precise positioning of streptavidin to the 12 biotin sites. Treatment of the biotinylated scaffold with 1,4-dithiothreitol (DTT) reduced the disulfide bond, thus removing the respective biotinylated units of the second class, giving rise to the pattern of streptavidin shown in Figure 13A. The subsequent interaction of the DTT-pretreated biotinylated surface with eosin in the presence of O_2 and under illumination, λ = 520 nm, resulted in the cleavage of the double bonds of the biotinylated units of class three, giving rise to a streptavidin-binding pattern on the noncleavable biotin staples. Figure 13B shows AFM images of the respective states: (I) after incubation with streptavidin, (II) following DTT reduction, and (III) eosin-treated streptavidin-modified origami template. The programmed positioning of proteins on the origami scaffold has been extended by predesigning three different functional tethers to the origami array. This was achieved by the linkage of an azide, an amino functionality, and an alkyne functionality to the origami array. The subsequent specific covalent linkage of an azide labeled with biotin to the alkyne units by a click reaction in the presence of copper(I)−THTA (tris-(1-[3-hydroxy-propyl]triazolyl-4-methyl)amine), the covalent attachment of a biotin-labeled *N*-hydroxysuccinimide activated ester (NHS-ester) to the amine functionalities, or the specific click-on reaction of a biotinylated alkyne to the azide tethers led to the specific modification of the origami array with the respective biotin label. The subsequent attachment of streptavidin (SA) to the biotin labels resulted in the ordered positioning of the protein on the DNA framework. Realizing that the different synthetic routes may be implemented to covalently link different proteins to the origami scaffold, one may anticipate that ordered structures consisting of intercommunicating proteins may be generated (Figure 13C).

A related study has implemented the origami nanostructure for the spatial positioning of proteins.[88] The biotin group, the chlorohexyl unit, and the benzylguanine groups were attached to specific stapled domains. Whereas the biotin binds streptavidin, the chlorohexyl functionalities associate specifically with haloalkane dehalogenase, known as the "Halo-Tag",[89] and the benzylguanine sites link specifically the O^6-alkylguanine-DNA-alkyltransferase (hAGT) known as the "Snap-Tag".[90] By the genetic engineering of proteins with the Halo-Tag or the Snap-Tag moieties, and the use of streptavidin−protein conjugates, the respective proteins were addressed to the appropriate recognition domains on the origami template. Another approach to construct one-dimensional and two-dimensional streptavidin (SA) nanoarrays on an origami scaffold has involved the construction of periodical nanometer-scale wells embedded in one-dimensional or two-dimensional DNA origami templates.[91] The M13 phage DNA was folded into a nanostructure using 267 staple strands to yield a rectangle consisting of 76 turns-long (theoretical length 260 nm) and 10 helices-wide (theoretical width of 30 nm) that include nine hollow sections (wells) exhibiting theoretical dimensions of 6.8 × 12 × 2.0 nm (Figure 14A). Each of the wells was modified with two biotin labels that allowed the association of SA. Figure 14B shows the AFM images corresponding to the periodically separated wells before and after the binding of SA (I and II, respectively). The precise positioning of the streptavidin at distances corresponding to the theoretically predicted separation, 28 ± 1 nm, was visualized.

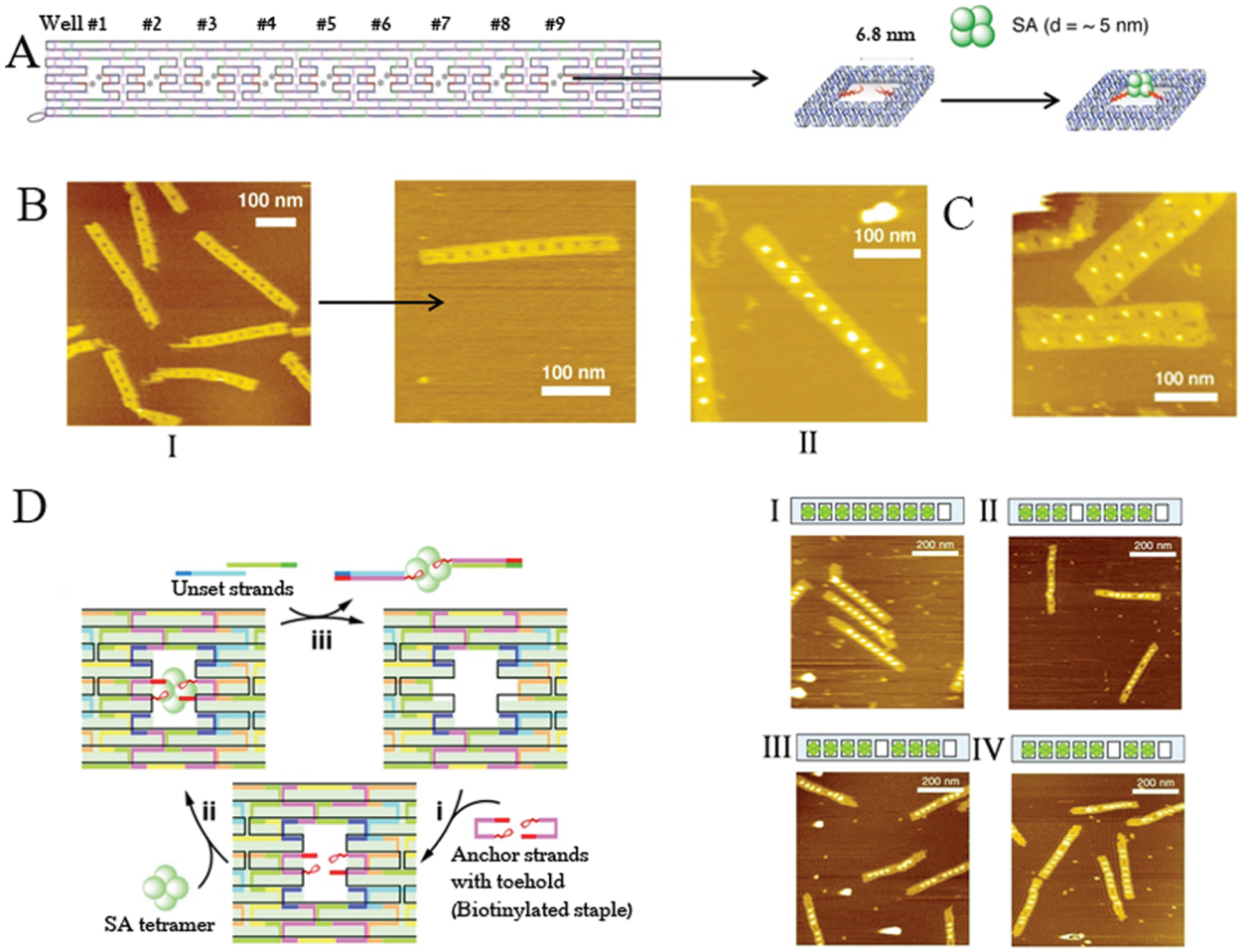

Figure 14. (A) Origami rectangular nanostructure consisting of nine wells, each modified with two biotin labels. Streptavidin was then selectively linked to the wells. (B) AFM images of the origami nanostructure (I) prior to the binding of streptavidin and (II) after the association of streptavidin to the wells. (C) AFM image of two origami subunits shown in (A) linked together by sticky-ends associated with the longitudinal domain of the nanostructure, and streptavidin bound in a zigzag configuration to the wells of the two origami nanostructures. Reprinted with permission from ref 91. Copyright 2009 Wiley-VCH. (D) Origami nanostructure consisting of wells functionalized each with different biotinylated nucleic acid tethers; sreptavidin was linked to the different biotinylated wells. By applying the strand-displacement principle, the selective removal of the streptavidin−biotin complex was achieved. Right: AFM images of (I) wells 1−8 occupied with streptavidin and (II−IV) selective removal of streptavidin from specific wells by strand displacement. Reprinted with permission from ref 92. Copyright 2010 Royal Society of Chemistry.

By the subsequent synthesis of two rectangles that included on their long edges complementary strands, the fabrication of two interhybridized rectangles, which included two parallel rows of wells, was achieved. The rectangles were designed, however, to include the biotin labels only on the even-numbered wells of one rectangle and on the odd-numbered wells of the second rectangle. This enabled the zigzag positioning of SA on the respective biotin-labeled origami composite (Figure 14C). The approach to assemble SA on periodically positioned wells constructed on an origami template was extended to yield the switchable binding and dissociation of SA to the wells (Figure 14D).[92] The well included two staple strands that hybridized with the complementary biotinylated strands. The association of SA to the biotin labels attached the protein to the well. The subsequent displacement of the biotinylated strand by a toehold mechanism removed the SA−biotin structure from the wells, leaving behind the functionalized wells for the secondary hybridization of the biotin-functionalized nucleic acid and the association of SA.

An intriguing origami-based three-dimensional nanostructure that represents a nanobox was constructed, and the opening of the lid of the box was demonstrated.[93] Albeit the reported box was not coupled to any protein, the hollow cavity inside the box, and the controllable opening of the lid, suggest the possible trapping and release of proteins or low-molecular-weight molecules to and from the box, as a future perspective of this nanostructure. M13 phage DNA was self-assembled using 220 staple strands into six different origami sheets (Figure 15A). The respective corners of each of the sheets included single toehold strands of appropriate complementarity that linked together the appropriate sheets. This arrangement enabled the self-assembly of the six-face box that generated a nanostructure with dimensions of 42 × 36 × 38 nm. The cryo-TEM images of the box are depicted in Figure 15B. The upper face of the box (the lid) was functionalized with a single-stranded nucleic acid complementary to a free nucleic acid strand tethered to the counterface. These two nucleic acids provided the lock−key mechanism for opening the box. (As the nucleic acid strand linked to the lid

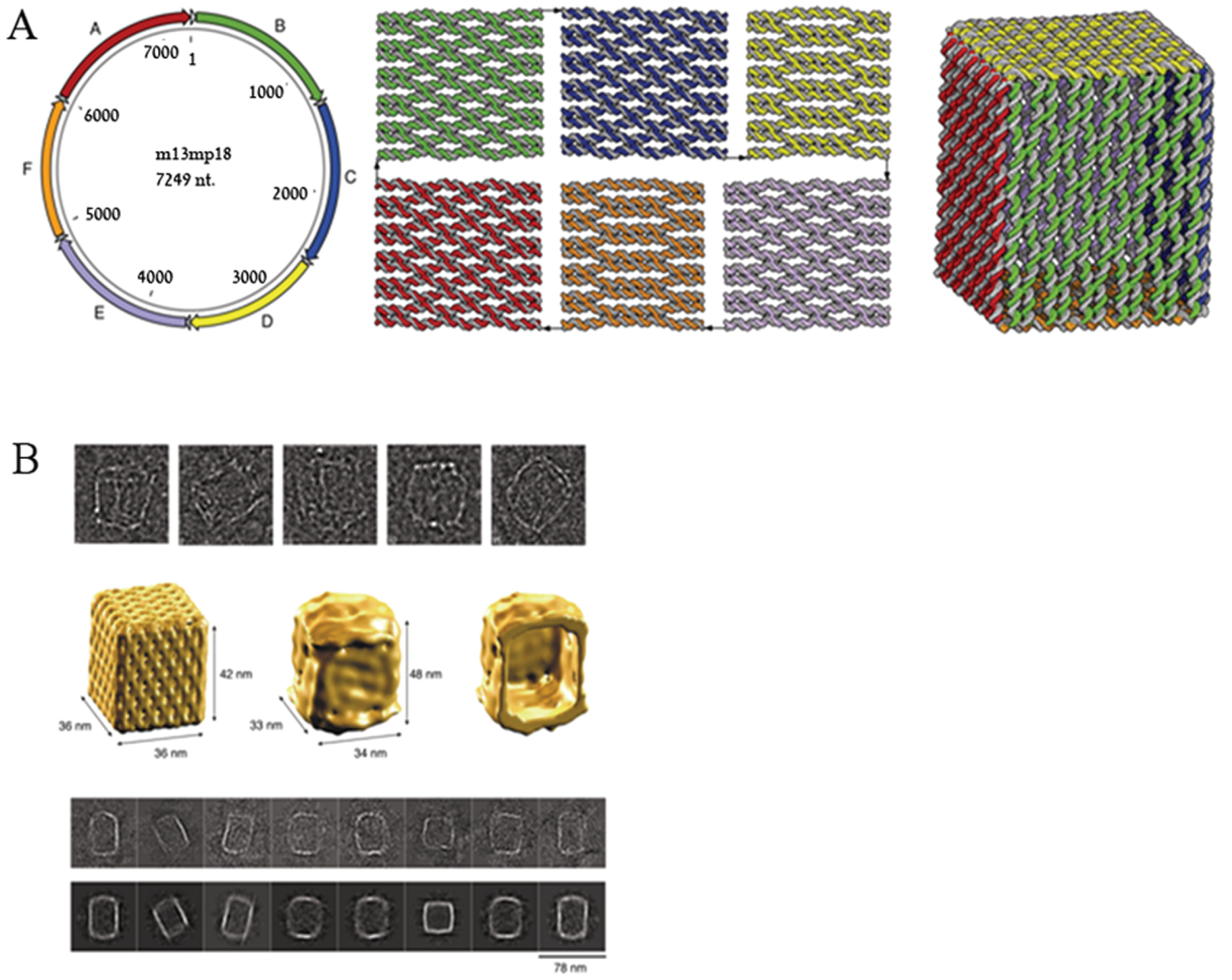

Figure 15. (A) Organization of six different origami sheets that include complementary domains that fold into a three-dimensional box by intersheets complementarities. (B) Cryo-TEM images of the resulting "box" nanostructure. Reprinted with permission from ref 93. Copyright 2009 Nature Publishing Group.

(key) hybridized to the lock associated with the counterface, which included a single-stranded toehold sequence, the application of an external strand that binds to the "key" strand associated with the lid results in strand displacement of the key–lock counterparts and the opening of the box). The opening of the box was characterized by following the fluorescence resonance energy transfer (FRET) between the key and lock elements. Such three-dimensional nanostructures may be implemented in the future as "smart containers" for controlled release of drugs.

5. SELF-ASSEMBLY OF DNA NANOPARTICLE NANOSTRUCTURES THROUGH HYBRIDIZATION OR DNA–PROTEIN INTERACTIONS

DNA has been used to program the assembly of 3D nanoparticle structures and even to prepare crystalline structures of NPs. 3D pyramidal arrangements of Au NPs have been prepared by the application of four different Au NPs that were each modified with a single nucleic acid strand exhibiting interparticle complementarities (Figure 16A).[94] The duplex DNA bridges provided a rigid linker for the self-assembly of 3D pyramids that included at their corners the Au NPs (Figure 16A and B). By applying four differently sized Au NPs, the programmed positioning of the NPs to form chiral 3D pyramids was demonstrated (Figure 16C).

DNA nanostructures were used as scaffolds for the dictated positioning of Au NPs (Figure 17).[95] The organic 1,3-bis(4-hydroxyphenyl) benzene unit was used as organic vertex to which different nucleic acids were covalently linked. By the use of three hybrid units consisting of the organic vertex and three different nucleic acids a, b, and c, a triangle-type nanostructure was generated through cross-linking of the hybrids with the complementary nucleic acids (Figure 17A). Similarly, by using four hybrid subunits (Figure 17B), a square-like DNA structure was formed upon cross-linking of the subunits by complementary nucleic acids. The subsequent ligation of the nanostructures hybridized by the auxiliary DNA linkers, followed by the separation of the duplexes and the separation of the single strands linked via the organic vertex, led to templates that included addressable single-stranded domains (Figure 17A and B). The hybridization of Au NPs modified with complementary nucleic acids a′, b′, and c′ to

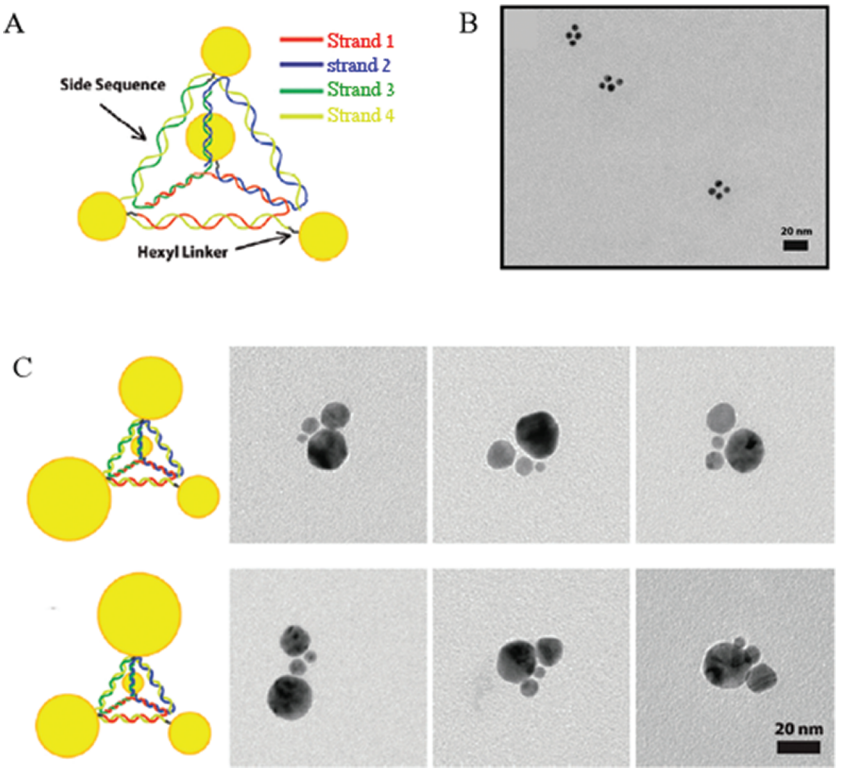

Figure 16. (A) Self-assembly of nucleic acid-functionalized Au NPs (5 nm) into a pyramidal nanostructure using complementary nucleic acids as rigidification units. (B) TEM image of the resulting pyramidal Au NPs assemblies. (C) Assembly of pyramidal DNA units consisting of differently sized Au NPs (5, 10, 15, and 20 nm) at the pyramid corners, and the respective TEM image. Reprinted with permission from ref 94. Copyright 2009 American Chemical Society.

the triangle template or Au NPs functionalized with the nucleic acids a′, b′, c′, and d′ complementary to the square-type template led to the precise positioning of the NPs on the presynthesized DNA scaffolds (parts C and D of Figure 17, respectively). By using differently sized Au NPs, the complexity of the resulting nanostructures was enhanced.

The aggregation of metallic NPs (e.g., Au NPs) through the linking of nucleic acid-functionalized NPs by bridging DNAs has been a widespread process for the development of numerous optical sensors.[96] Recently, the controlled aggregation of nucleic acid-modified Au NPs led to the formation of crystalline nanostructures consisting of the NPs.[97] One face-centered cubic crystalline structure was generated as outlined in Figure 18A. Au NPs were functionalized with the nucleic acid (**27**). The complementary nucleic acid (**28**) that included palindromic single-stranded tethers was hybridized to the particles. The palindromic tethers linked to different Au NPs bridged the NPs, so that the face-centered cubic (fcc) nanostructure was formed. Alternatively, a body-centered cubic (bcc) crystalline structure of Au NPs was generated as outlined in Figure 18B. Two kinds of DNA-functionalized Au NPs were synthesized by the hybridization of complementary nucleic acids **29** or **30** with the **27**-functionalized Au NPs. These NPs include different single-stranded tethers of interparticle complementarities. Upon the bridging of the two kinds of Au NPs, the bcc crystalline structures were formed.

DNA nanotubes with longitudinal structural variations were prepared and used to load and release a nanocargo.[98] DNA triangles of two different sizes (edge lengths of ~7 nm for **31** and ~14 nm for **32**) were used to construct triangular-based nanotubes, by the hybridization with nine double-stranded linking strands (Figure 19A). The resulting nanotubes were composed of alternate small and large triangles that were bridged to form small and large capsules. AFM and TEM analyses demonstrated the formation of micrometers-long DNA nanotubes (Figure 19B). The resulting DNA nanotubes entrapped and released Au NPs. Figure 19C outlines AFM and TEM images of DNA nanotubes that include the encapsulated 15 nm Au NPs. Citrate-stabilized Au NPs (15 nm) were introduced into the nanotubes within the process of "glueing" together of the triangles **31** and **32**, through hybridization, and the formation of the nanotubes. One may see the linear organization of the gold NPs that is achieved with the approximate spacing of ca. 100 nm separating the large capsules comprising the nanotubes. The Au NP-loaded nanotubes were then implemented as carriers for the directed release of the Au NPs "cargo" units. Addition of a single-strand nucleic acid that hybridizes with the bridging duplex units linking the triangle elements resulted in strand displacement and the disconnection of the rigid tubes, leading to the release of the encapsulated NPs.

The successful eliciting of DNA sequences that specifically bind to proteins (aptamers) provides a means to construct DNA−protein nanostructures. For example, two different oligonucleotide sequences (aptamer α and aptamer β) were reported to bind two different distinct domains of thrombin. This property was used to self-assemble linear or branched two-dimensional thrombin−DNA nanostructures[99] (Figure 20A). The oligonucleotide **33** includes at its two ends the sequences corresponding to aptamer α and aptamer β for thrombin. Thus, in the presence of thrombin, the oligonucleotide **33** acts as a

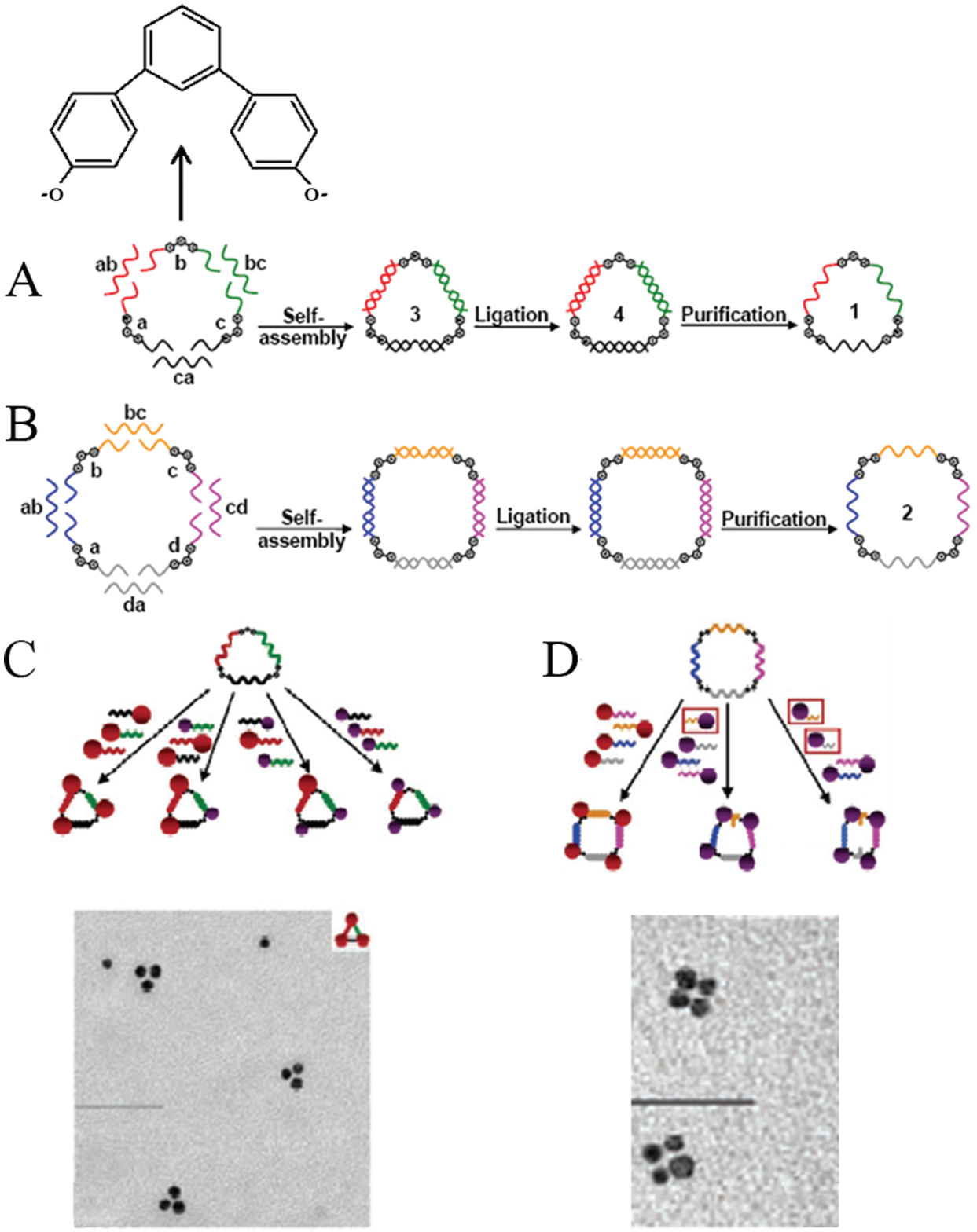

Figure 17. (A) Preparation of a DNA triangle that includes three synthetic vertices. Each of the vertices was functionalized by two nucleic acids. The three vertices were hybridized into the triangle configuration, and the nucleic acids associated with counter-vertices were ligated. After removal of the rigidifying hybridized nucleic acid, the single-stranded triangle was purified. (B) Preparation of a square DNA using an analogous procedure outlined in (A). (C) Functionalization of the triangle DNA with Au NPs modified with nucleic acids complementary to the sides of the triangle, and the respective TEM image. (D) Functionalization of the square DNA with Au NPs modified with nucleic acids complementary to the side of the DNA template, and the respective TEM image. Reprinted with permission from ref 95. Copyright 2007 American Chemical Society.

dx.doi.org/10.1021/cr200104q |*Chem. Rev.* 2012, 112, 2528–2556

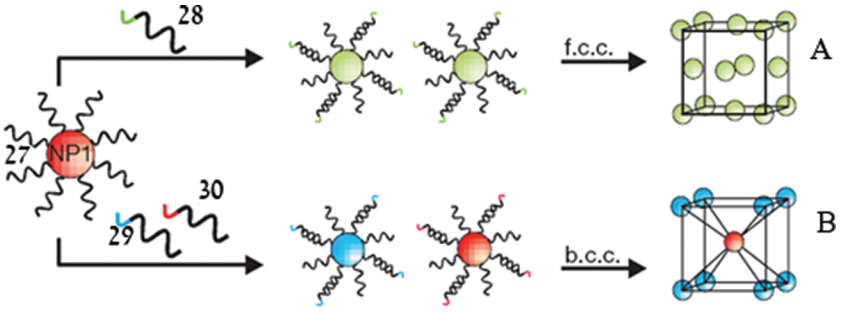

Figure 18. Self-organization of nucleic acid-functionalized Au NPs into crystalline nanostructures: (A) a fcc structure and (B) a bcc structure. Reprinted with permission from ref 97a. Copyright 2008 Nature Publishing Group.

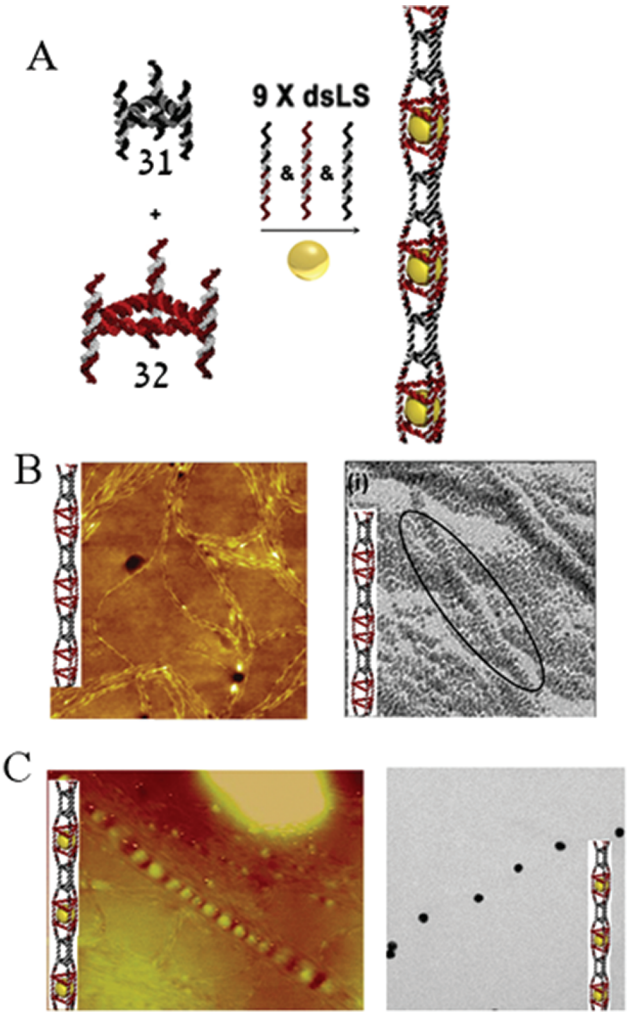

Figure 19. (A) Self-assembly of DNA nanotubes with incorporated Au NPs by the cross-hybridization of two-sized DNA triangles with a tethered nucleic acid and a set of nine nucleic acid linkers. (B) AFM and TEM images of the nanotubes without Au NPs. (C) AFM and TEM images of the Au NPs encapsulated into the DNA tubes. Reprinted with permission from ref 98. Copyright 2010 Nature Publishing Group.

"glue" that self-assembles the thrombin-binding aptamer units/thrombin into a wire. Similarly, a mixture of the bifunctional α/β bis-aptamer oligonucleotide **33** and the tripod oligonucleotide **34**, which includes three aptamer α head groups led, in the presence of thrombin, to the self-assembly of branched thrombin/thrombin-binding aptamer-bridged nanostructures. Figure 20B depicts AFM images and cross-sectional analysis of a linear DNA−protein wire, revealing a height of ca. 2.5 nm.

Similarly, aptamers against low-molecular-weight substrates, such as cocaine, adenosine monophosphate, and more, can be generated by selection/amplification procedures.[17,40,100] It was demonstrated that the specific aptamer sequences against low-molecular-weight substrates can be fragmented into subunits that self-assemble into the aptamer subunits−substrate supramolecular structure.[101] This property was implemented to develop optical or electrochemical aptasensors for the low-molecular-weight substrates.[102] The self-assembly of aptamer fragments and their substrates to the respective supramolecular complex was used to self-assemble composite DNA−aptamer hybrid nanostructures that were subsequently used as scaffolds for the programmed positioning of two different enzymes[103] (glucose oxidase (GOx) and horseradish peroxidase (HRP)) (Figure 21A). The intramolecular hybridization of oligonucleotides **35** and **36** by the capping nucleic acids **37** and **38** yielded the capped circular substrates **35**/**37** and **36**/**38**. The oligonucleotides **39** and **40** include domains complementary to the nucleic acid **37** and **38** and specific domains corresponding to the fragmented subunits of the aptamer against cocaine **41**. In the presence of cocaine, the supramolecular hybrid polymeric nanostructure consisting of the circular DNAs I and II bridged by the aptamer−cocaine complexes is formed path A Figure 21B shows an AFM image of the respective wire. The height of the wire is ca. 3.5 nm. The increased height was attributed to the flexibility of the aptamer−DNA circle units and to the fact that the rings might have collapsed to compact structures of increased heights. The bridged aptamer−circular DNAs nanostructure was further implemented to specifically bind two different enzymes, GOx and HRP, to the scaffold (Figure 21A, path B). In this nanostructure, the circular DNAs were capped by nucleic acids that were covalently tethered to the two different enzymes. The hybrid bienzyme DNA/aptamer nanostructure enabled the effective activation of the enzyme cascade, as previously described (see section 2).

Another method to self-assemble DNA scaffolds for the directed positioning of enzymes or metallic nanoparticles has involved the self-assembly of polycatenated DNA rings[104] (Figure 22A). The single strands **42** and **43** included complementary domains that upon hybridization resulted in the formation of interconnected DNA strands. The ligation of the 3′ and 5′ ends of the rings resulted in polycatenated rings of DNA. Figure 22B depicts the AFM images of wires of DNA, exhibiting a height of 2 nm, corresponding to double-stranded DNA.

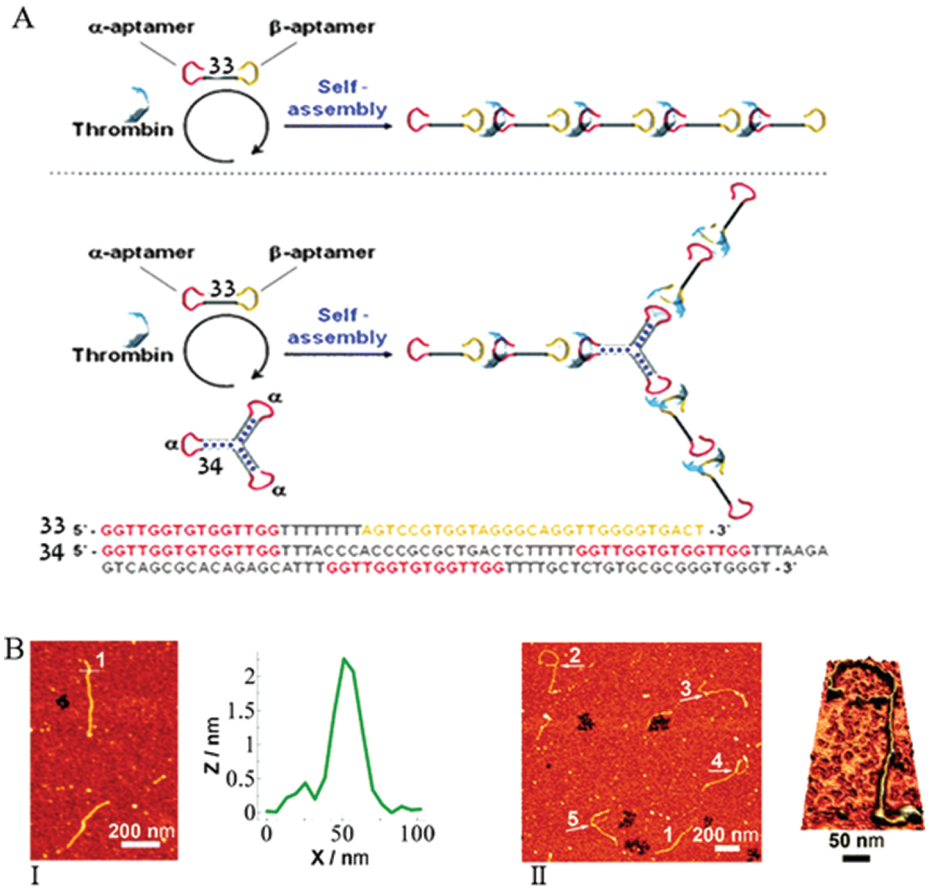

Figure 20. (A) Self-assembly of linear or branched thrombin/bis-aptamer nanowires. (B) AFM images of the linear (I) and branched (II) nanowires. Reprinted with permission from ref 99. Copyright 2008 Royal Society of Chemistry.

One can observe the catenated DNA rings, comprising the DNA nanostructure. The polycatenated DNA included single-stranded rails that provided hybridization sites for tethering proteins or metallic nanoparticles. By designing the rails to contain thrombin-binding aptamer units, tetramethylrhodamine (TAMRA)-labeled thrombin was attached to the rails of the polycatenated structure, to form protein−DNA hybrid nanostructures (Figure 22 A and C).

Single-sranded DNA chains with appropriate complementarities provided a means to self-assemble hexagon-like DNA strips.[105] For example, Figure 23A shows the use of two DNA chains **44** and **45** that self-assemble into a two-hexagon strip. Similarly, upon application of the four hexagons **46**−**49**, which include the appropriate complementarities, the self-assembly of four-hexagon-based strips was performed. Micrometer-long DNA strips, with an average height of ca. 2 nm, were imaged (Figure 23B). The hexagon subunits included single-stranded nucleic acid tethers at the edge of the respective strips. These tethers provided anchoring sites for the coupling of enzymes, while dictating the distance separating the enzymes and thus controlling the effectiveness of communication between the enzymes on the DNA scaffolds. The enzymes glucose oxidase (GOx) and horseradish peroxidase (HRP) were modified by nucleic acids **50** and **51**, which are complementary to the tethers associated with hexagons **45** and **44** or **49** and **46**, respectively (Figure 23C). The bienzyme cascade, where GOx mediated the oxidation of glucose by O_2 to yield gluconic acid and hydrogen peroxide (H_2O_2), and the subsequent HRP-catalyzed oxidation of 2′2′-azino-bis[3-ethylbenzthiazoline-6-sulfonic-acid] ($ABTS^{2-}$) by H_2O_2 was activated on the respective DNA scaffolds. The biocatalytic cascade generated the colored product $ABTS^{\bullet-}$, which reflected the effectiveness of the bienzyme biocatalytic transformation. Effective interenzyme communication, and the activation of the enzyme cascade, were observed on the DNA hexagon strips (Figure 23D, curves a and b). The enzmes, at the same concentrations, in the absance of DNA, as in the presence of a Breign, non-organizing, DNA did not communicate with one another (Figure 23D, curves c and d), implying that their connection and ordering on the DNA scaffold established the interenzyme contact. Also, the spatial separation of the two enzymes on the four hexagon strips led to a ca. 20% less efficient activation of the bienzyme cascade, revealing the significance of proximity between the enzymes for an effective biocatalytic cascade. Similarly, the enzyme glucose dehydrogenase (GDH) and its N-(1)-(2-aminoethylnicotinamideadenine dinucleotide) (NAD^+) cofactor were assembled on the two hexagon DNA scaffold (Figure 23E). Although the enzyme GDH was functionalized with a nucleic acid complementary to the tether unit **45**, the NAD^+ cofactor was functionalized with single-stranded DNAs of variable lengths that included a domain complementary to the tether **44**. The oxidation of glucose to gluconic acid by the NAD^+ cofactor yields the reduced NADH cofactor, and this reduces methylene blue (MB^+) to the colorless reduced dye, MB, thus providing a color signal for the cofactor-mediated

dx.doi.org/10.1021/cr200104q |*Chem. Rev.* 2012, 112, 2528–2556

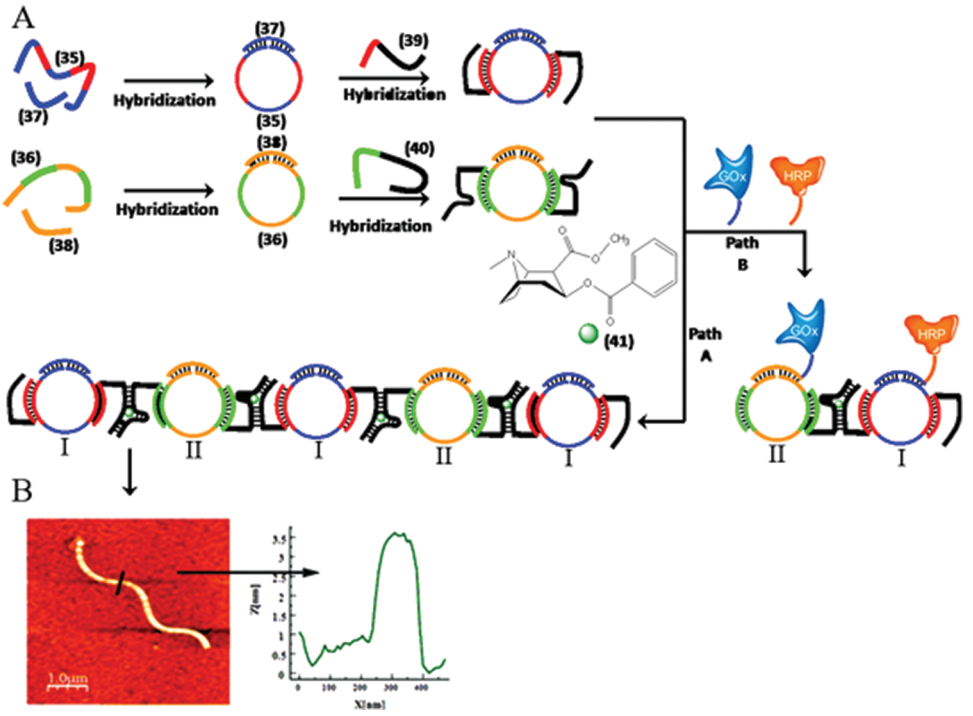

Figure 21. (A) Self-assembly of circular DNA units by the selective hybridization of anticocaine aptamer subunits to two different DNA circles and the programmed conjugation of the circles by cocaine (path A). The selective association of the enzymes glucose oxidase and horseradish peroxidase to the different circles activates the bienzyme cascade (path B). (B) AFM image of the cocaine-conjugated circular DNA nanowire. Reprinted with permission from ref 103. Copyright 2009 American Chemical Society.

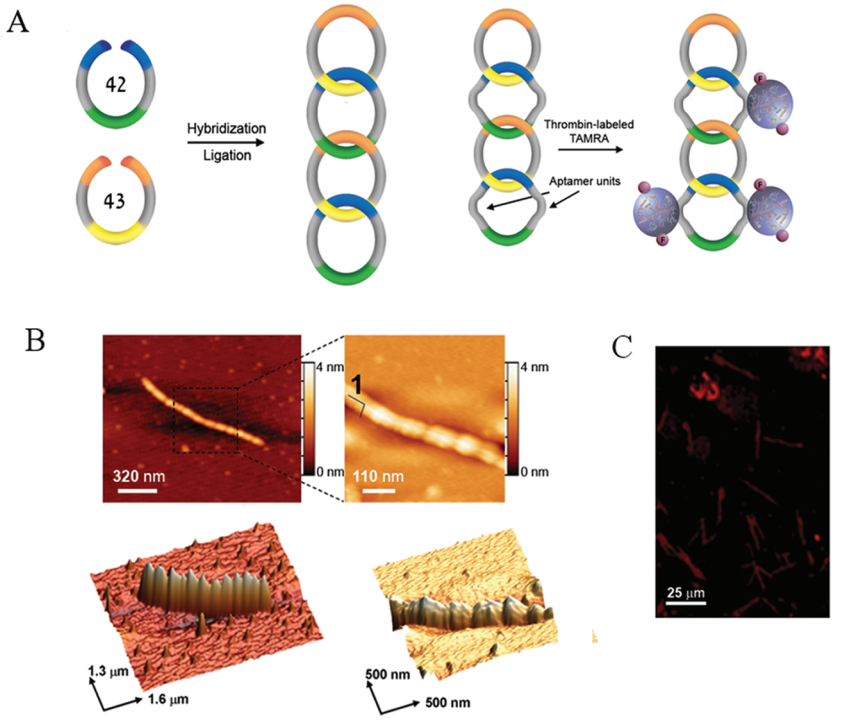

Figure 22. (A) Synthesis of catenated DNA nanowires. (B) AFM images of the catenated DNA nanowires. (C) Association of TAMRA-labeled thrombin to the aptameric rails of the catenated DNA nanowires and the respective confocal microscopy image of the nanowires. Reprinted with permission from ref 104. Copyright 2008 National Academy of Sciences.

biocatalyzed oxidation of glucose on the DNA scaffold (Figure 23F). While NAD^+ linked to the DNA scaffold with a short chain was inefficient in the activation of the cofactor-mediated biocatalytic transformation, elongation of the DNA tether

dx.doi.org/10.1021/cr200104q |*Chem. Rev.* 2012, 112, 2528–2556

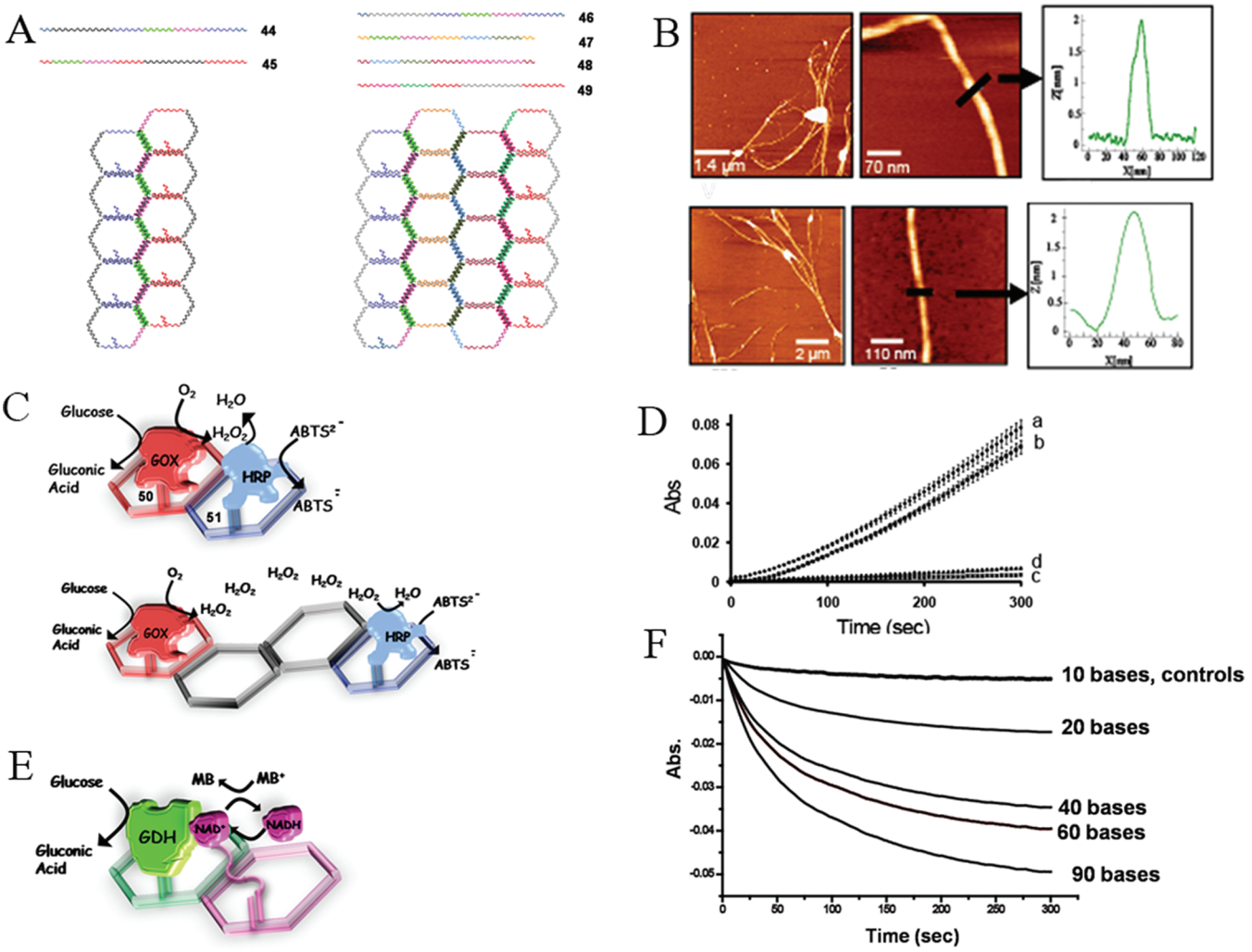

Figure 23. (A) Self-assembly of protruding nucleic acid-functionalized strips consisting of "two-hexagon" and "four-hexagon" building units. (B) AFM images of the resulting two-hexagon and four-hexagon strips. (C) Programmed attachment of the enzymes glucose oxidase (GOx) and horseradish peroxidase (HRP) to the protruding nucleic acids, and the activation of the bienzyme cascade in the organized nanostructuctures. (D) Colorimetric analysis of the bienzyme cascade in the two-hexagon/enzyme (a) and the four-hexagon/enzyme (b) nanostructures. Curves (c) and (d) correspond to control experiments where the bienzyme cascade was examined in the absence of DNA (c) or in the presence of the foreign calf-thymus DNA (d). (E) Activation of the NAD^+-dependent glucose dehydrogenase (GDH) on the two-hexagon DNA strips by the programmed assembly of the NAD^+ cofactor and GDH on the nanostructure. The NAD^+ cofactor was tethered to the DNA scaffold by nucleic acids of variable lengths. (F) Colorimetric assay of the GDH biocatalytic activity in the presence of the NAD^+ linked to the scaffold by different tether lengths. Reprinted with permission from ref 105. Copyright 2009 Nature Publishing Group.

improved the contact between the cofactor and the enzyme, and the optimal biocatalytic transformation was observed upon using a chain of 90 bases.

6. DNA NANOSTRUCTURES AS TEMPLATES FOR THE BOTTOM-UP FABRICATION OF NANODEVICES

The continuous effort to miniaturize electronic circuits is a challenging holy grail in modern science. Although the last 50 years demonstrated the increase of the density of electronic computing elements, which is doubled every 2 years (Moore's law), it is anticipated that the lithographic miniaturization method will reach limiting values. Accordingly, research efforts in the past decade suggested an alternative bottom-up approach, where molecules or macromolecules act as templates for the deposition of nanocircuits. The nanodimensions of proteins or DNA, the structural information encoded in these materials, and the available chemical means to attach metallic or semiconductor nanoparticles to these biopolymers enables the growth of microcircuits on the biomaterials acting as organizing templates. For example, amyloid nanotubes served as scaffolds for the deposition of silver and the generation of silver nanowires.[106] Similarly, the enzymes glucose oxidase and alkaline phosphatase were patterned via dip-pen nanolitography on surfaces and served as nanobioreactors for the electroless deposition of different metals.[45]

DNA provides, however, unique features for the application of the biopolymer as a template for the organization of nanoscale electronic circuitries and nanodevices. The availability of DNA of controlled lengths, predesigned base sequence, and nanoengineered geometrical topologies enables the programming of the DNA into functional matrices, acting as scaffolds for the bottom-up organization of nanostructures. Also, the availability of specific enzymes that react with nucleic acids, such as polymerase,

dx.doi.org/10.1021/cr200104q |*Chem. Rev.* 2012, 112, 2528–2556

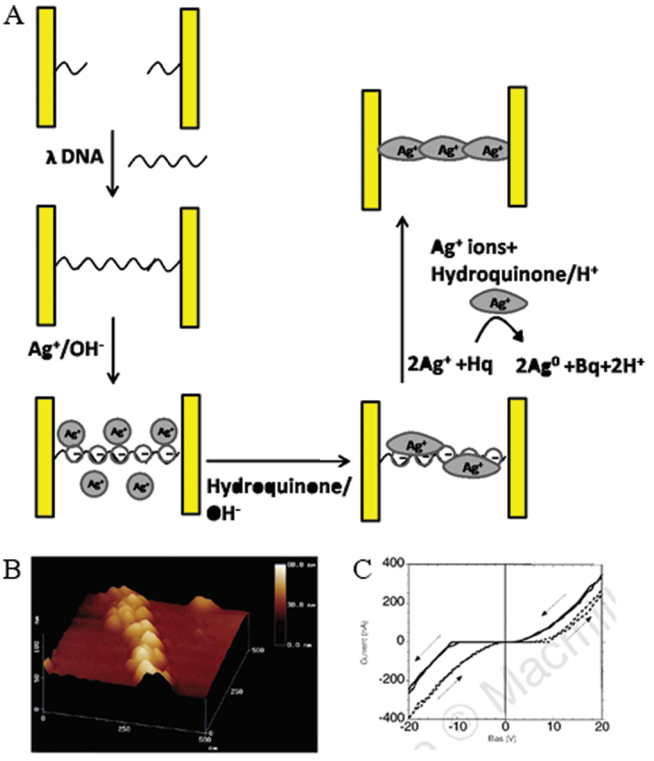

Figure 24. (A) Bridging microelectrodes with a Ag nanowire deposited on a DNA template. (B) AFM image of the resulting nanowire. (C) Representative I−V curves of different Ag nanowires bridging the microelectrodes. Reprinted with permission from ref 107. Copyright 1998 Nature Publishing Group.

telomerase, sequence-specific endonucleases, DNA recombination proteins (such as RecA), or nicking enzymes that cleave DNA, provide unique nanoscale biological tools for manipulating and molding of DNA structures. Also, the sequence-specific interactions of proteins with DNA domains enable the biochemical "patterning" of DNA polymers with domains of predesigned chemical reactivities. Not surprisingly, DNA nanostructures find growing interest as templates for the assembly of nanocircuits and nanodevices. The metallization of DNA templates, or the specific attachment of semiconductors to DNA scaffolds, attracted substantial efforts directed to the fabrication of nanoelectronic systems.

A silver-coated phage λ DNA metallic nanowire was used to bridge the gap between two microelectrodes and to construct a conductive nanowire[107] (Figure 24A). The two electrodes were modified with short DNA strands of 12 bases each, which were complementary to the 5′ and 3′ end of the phage λ DNA. Subsequently, the phage λ DNA was hybridized to the short nucleic acids linked to the microelectrodes, and Ag^+ ions were associated with the phosphate groups of the DNA scaffold. The primary reduction of the Ag^+ ions to Ag^0 nanoclusters, linked to the DNA template, by hydroquinone under basic conditions, followed by the catalytic, electroless enlargement of the Ag^0 nanoclusters by the deposition of silver on the nanoclusters, led to the formation of continuous Ag^0 nanowire (Figure 24A and B). Figure 24C depicts the I−V curves of the resulting metallic nanowire, revealing a nonlinear behavior and demonstrating potential regions of insulating properties of variable widths, exhibiting different on-set potentials for the generation of the currents. The non-ohmic I−V curves were attributed to defects in the contacts between the metallic nanoclusters consisting of the nanowires that introduced overpotentials for charge transport.

The concept of metallization of DNA templates and the formation of metallic nanowires was further extended to design addressable conductive domains on DNA templates and to fabricate nanoscale transistor devices.[108] To reach this goal, the RecA bacterial protein that participates in gene repair and homologous recombination[109] was implemented as an organizing element of the nanodevice (Figure 25A). A single-stranded DNA was complexed with the RecA protein, and the resulting complex was incorporated into an addressed domain of a long duplex DNA through homologous recombination, to yield a duplex DNA patterned with RecA. The subsequent binding of the biotinylated anti-RecA to the protein, followed by the attachment of streptavidin-modified carbon nanotubes, addressed the semiconductor carbon nanotubes onto the duplex DNA template. The further modification of the protein-free duplex DNA domains with Ag^+ ions, their reduction to nanoclusters, and the electroless catalytic deposition of Au on the Ag nanoclusters, yielded electrical contacts that were separated by the semiconductor carbon nanotubes, acting as a gate. Figure 25B depicts the SEM image of the resulting nanodevice. The performance of the resulting field-effect transistor is depicted in Figure 25C, where the source-to-drain currents at variable source-to-drain potentials (V_{DS}) and different gate potentials (V_G) are depicted.

A related approach was applied to fabricate nanoscale metallic nanowires that bridge two microelectrodes.[110] The mutated RecA protein that included at its c-terminus a cysteine residue was functionalized with maleimide-modified Au NPs (1.4 nm). The resulting Au NPs-functionalized RecA was complexed to a single-stranded DNA and deposited on a gap separating two electrodes. The subsequent enlargement of the Au NPs with Au by an electroless deposition process yielded continuous wires exhibiting diameters in the range of 80−500 nm. Figure 26A shows the SEM image of the resulting nanowire that reveals an ohmic-type conductivity (Figure 26B).

Single strands of DNA acted as templates for growing metallic or semiconductor nanowires and their incorporation as circuitry elements for probing the charge transport properties of the nanodevices. For example, the 48,502 base λ DNA was deposited on a gap separating two electrodes.[111] The association of Pd^{2+} ions with the phosphate residues followed by the reduction of the ions, with a mixture of sodium citrate, lactic acid, and dimethylamine borane, generated Pd^0 nanoclusters on the DNA template. The application of repeated association of Pd^{2+} ions and reduction cycles led to the formation of continuous metallic nanowires (Figure 27A) that revealed ohmic conductivity (Figure 27B).

A related approach has implemented the λ DNA as a template to grow CdS semiconductor nanowires.[112] The DNA was interacted with Cd^{2+} ions that associated to the phosphate units. The reaction of the Cd^{2+}−DNA hybrid with Na_2S yielded CdS nanoclusters on the DNA template. The repeated deposition of Cd^{2+} ions and reaction with sulfide anions generated continuous CdS nanowires (Figure 28A), and these were assembled on a gap that separated two electrodes using a combing technique (Figure 28B). The I−V curves of the nanodevices revealed nonlinear behavior with insulating regions and onset potential, exhibiting conductivity features characteristic to semiconductors.

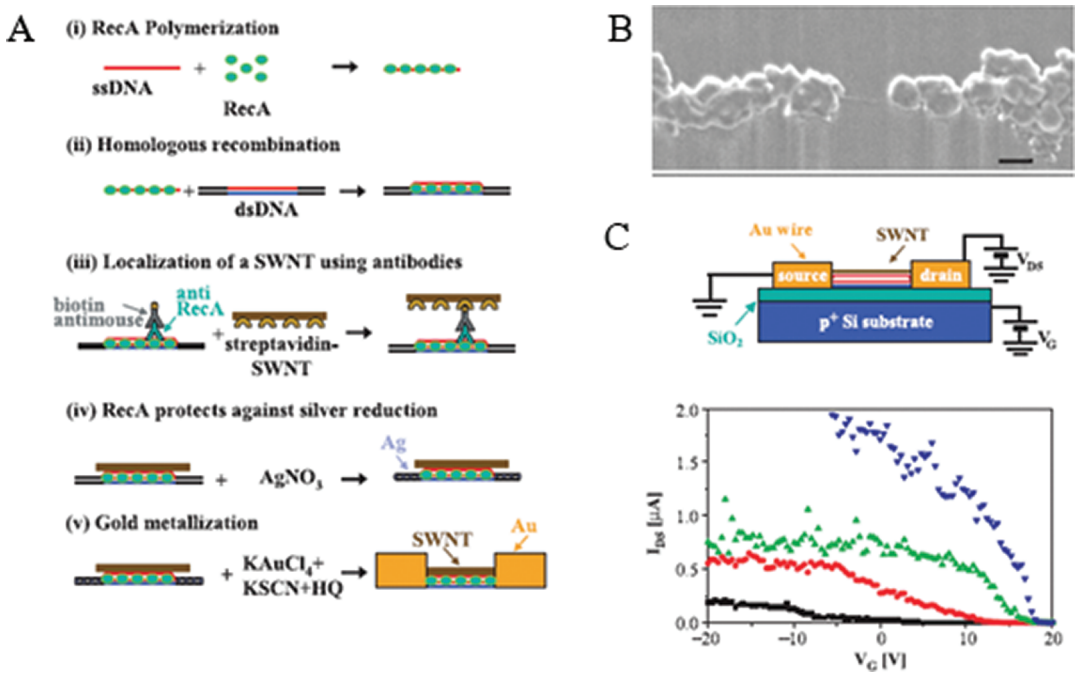

Figure 25. (A) Stepwise assembly of a nanotransistor device by the ordered deposition of carbon nanotubes on Ag metallic patterns generated on a DNA template. (B) SEM image of a carbon nanotube bridging the Ag nanowires deposited on the DNA template. (C) Schematic transistor configuration of the resulting nanotransistor and experimental I−V curves using different source-drain potentials. Reprinted with permission from ref 108. Copyright 2003 American Association for the Advancement of Science.

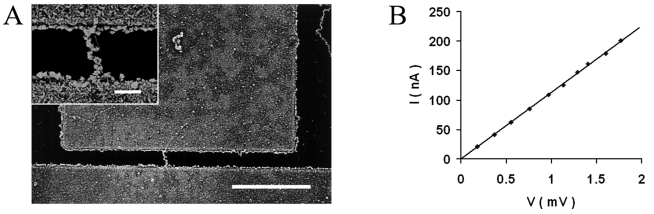

Figure 26. (A) SEM image of a Au nanowire bridging two microelectrodes that were generated by the catalytic enlargement of Au NPs associated with a DNA template. (B) I−V curve of the resulting nanowire. Reprinted with permission from ref 110. Copyright 2005 American Chemical Society.

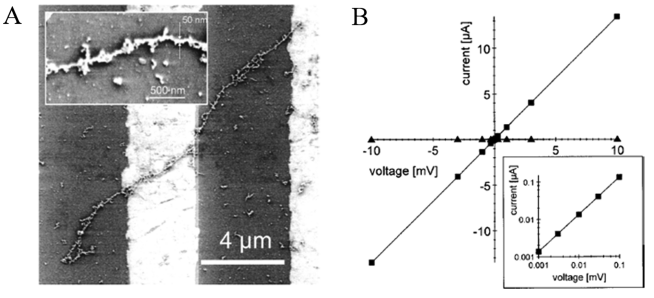

Figure 27. (A) SEM image of a Pd° nanowire synthesized on λ DNA template that bridges two microelectrodes. (B) I−V curve of the resulting Pd° nanowire. Reprinted with permission from ref 111. Copyright 2011 American Institute of Physics.

The effect of light on the photoconductivity of the device was not examined and remains an interesting topic for further research.

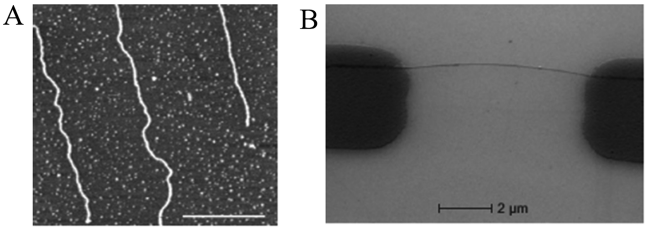

Figure 28. (A) AFM image of CdS nanowires generated on a λ DNA template. (B) SEM image of the CdS nanowire bridging two microelectrodes. Reprinted with permission from ref 112. Copyright 2007 Wiley-VCH.

A different approach to assemble conductive metallic nanowires on DNA templates used self-assembled DNA scaffolds for the deposition of metals.[113] Three-helix bundle tiles were assembled into bundles of nanotubes, and Ag^+ ions were linked to the phosphate groups. The ions were reduced to Ag° nanoclusters using glutaraldehyde as a reducing agent, followed by the enlargement of the Ag° nanoclusters to metallic nanowires using the Ag°-catalyzed reduction of Ag^+ by hydroquinone. Metallic micrometer-long nanowires exhibiting widths of 20−50 nm were formed. The resulting metallic nanowires were deposited in between a gap of electrodes, and the I−V curves of most of the metallic nanowires showed an ohmic behavior revealing resistances of 1.2−1.4 kΩ. The apparent high resistivity of the Ag nanowires as compared to bulk silver (1.6×10^{-8} Ω·m^{-1}) may be attributed to nanoscale defects that perturb the charge transport through the metallic nanowire. Similarly, DNA nanotubes were assembled from triple-crossover molecules and were further coated with silver.[114] Two different triple-crossover tiles (TX) of DNA **U** and **V** that included complementary sticky-ends

dx.doi.org/10.1021/cr200104q |*Chem. Rev.* 2012, 112, 2528–2556

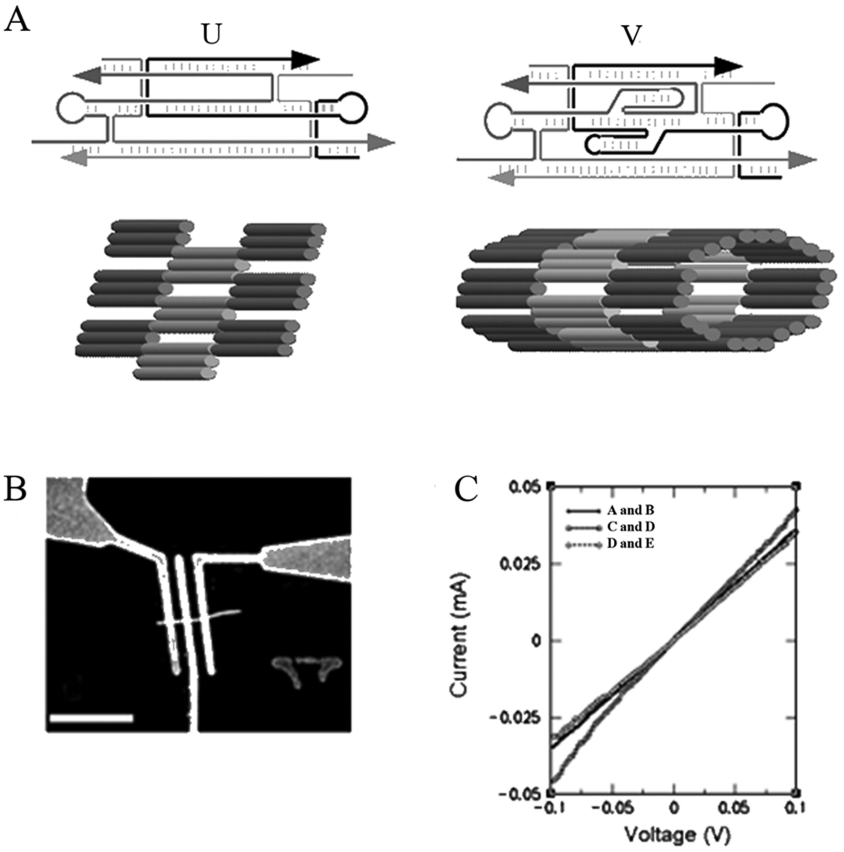

Figure 29. (A) Self-assembly of a DNA nanotube using two different TX tiles. (B) SEM image showing the silver-coated DNA tube deposited on an array of microelectrodes. (C) I−V curves of three different Ag° nanowires deposited on the microelectrodes. Reprinted with permission from ref 114. Copyright 2004 National Academy of Sciences, USA.

were used to self-assemble the DNA nanotubes, through the formation of sheets, that folded into nanotubes (Figure 29A). The TX nanotubes were then metalized by silver, using glutaraldehyde as a reducing agent. The resulting metallic nanotubes exhibited dimensions of ~35 nm in height, ~40 nm in width, and up to 5 μm in length. Chromium/gold electrodes were then patterned onto the nanowires by electron-beam lithography. Figure 29B shows a SEM image of the DNA metallic nanotubes-based device. I−V measurements were conducted on these devices with various gap distances: 180, 80, and 100 nm. The measurements revealed mostly ohmic behavior with resistances of 2.8, 2.35, and 2.82 kΩ, respectively, at a potential of 0.1 V at room temperature (Figure 29C).

7. CONCLUSIONS AND PERSPECTIVES

Impressive advances were accomplished in the past 10 years in the area of DNA nanotechnology and self-assembly of DNA−proteins or DNA−nanoparticle nanostructures. Versatile methods to assemble 1D, 2D, and 3D DNA−protein or DNA−nanoparticle systems were developed. These include the 1D organization of hybrid nanostructures by the implementation of the rolling circle amplification process (RCA), the ligation of interhybridized quasi-circular DNA strands to form catenated circular DNA polymers, by the self-organization of cDNA strands. 2D and 3D DNA−protein or DNA−nanoparticle structures were assembled by the application ingenious DNA−"tile" constructs as building blocks for the formation of programmed 2D arrays that upon folding generated 3D tubes. Similarly, the dictated origami folding, where a viral DNA is folded by appropriate "staple" units, proved to be a versatile method for the computer-aided formation of 2D or 3D nanostructures. Also, large capsules of DNA−NP nanotubes were generated through the directed polymerization of predesigned DNA-triangle subunits by complementary nucleic acids acting as "glue". Precise positioning of proteins or NPs onto the resulting nanostructures was realized by the programmed functionalization of the self-assembled nanostructures with protruding nucleic acids, chemically reactive groups, or ligands that control the binding of the components through hybridization, covalent bonds, or supramolecular affinity interactions. Although substantial progress was achieved in the nanoengineering of hybrid DNA nanostructures, challenging fundamental and practical issues are still ahead of us. Although the formation of the DNA nanostructures and the spatial positioning of proteins/NPs on the systems were demonstrated, the resulting systems are imperfect and include unavoidable defects. Thus, the development of error-correction methods is an essential future requisite. Further exciting opportunities in the area of DNA hybrid nanostructures would involve the development of signal-triggered systems, where chemical, electrochemical, or photochemical stimuli reversibly interconvert the topologies of DNA hybrid nanostructures. Such nanostructures may find important applications for the controlled delivery, uptake, and release of substrates.

The major challenges include, however, the identification of potential applications of hybrid DNA nanostructures. The use of

a DNA scaffold for the bottom-up templated synthesis of metallic or semiconductor nanowires for the miniaturization of electronic circuitry has been demonstrated. Nonetheless, the chemical growth of electronic circuitry on DNA templates is not free of limitations. Defects in the resulting nanowires were found to perturb the charge transport through the circuitries. The improvement of the quality of the nano-objects and the theoretical understanding of the effects dominating charge transport through the nanowires are desirable goals. The fabrication of high-throughput, defect-free, nanoscale devices based on DNA hybrid nanostructures would require, however, the development of surface-patterning methods for addressing the nanocircuitries. Alternatively, one might envisage the future design of DNA templated metallic or semiconductor nanowires that are integrated with motor proteins. The fueled motility of such nanowires on patterned tracks on surfaces could lead to the autonomous assembly of complex circuitries on surfaces. In fact, the ability to move metallic nanowires on surfaces by means of the actin/myosin motor protein and ATP has been demonstrated,[115] and similar principles may be adapted to move hybrid DNA nanostructures on surfaces.

Hybrid DNA−proteins or DNA−NP nanostructures hold great promise for other applications. Such nanocomposites may find different uses in nanomedicine. The encapsulation of therapeutic drugs in DNA tubes or DNA nanoboxes may provide nanoscale containments for carrying drugs and their slow release. Similarly, NPs encapsulated in DNA nanostructures might be useful vehicles for in vivo imaging or thermal destruction of tumor cells. Although such exciting ideas float around, fundamental issues, such as crossing cell boundaries by the DNA structures, triggered release of the encapsulated substrates, and stabilization of the DNA nanostructures in biological fluids or cells, need to be resolved. A further challenging path to implement DNA−protein or DNA/NPs would involve the control of chemical reactions through the spatial positioning of reactants on DNA templates. Recently, control over the reactivity of a bienzyme cascade, or a cofactor-enzyme biotransformation by means of DNA nanostructures, was demonstrated.[30b,42,103,105] This suggests that biocatalytic transformations, and specifically, artificial enzyme networks, might be engineered by the spatial positioning of biocatalysts on 1D, 2D, or 3D DNA nanosystems. Furthermore, protein or nanoparticle arrangements on DNA scaffolds may act as functional nanoarchitectures for light harvesting and solar energy conversion. The photosynthetic reaction centers provide a unique apparatus for the effective collection of light and its utilization for vectorial electron transfer accompanied by efficient charge separation. The precise positioning of photosensitizer and electron-acceptor chains on DNA nanostructures may lead to such photosynthetic devices.[30a] Finally, the integration of DNA machines,[25−30] such as walkers or a crane on programmed "playgrounds" of DNA arrays, might be useful to assemble nanoscale machines carrying objects in dictated directions.

The topic of DNA−protein or DNA−nanoparticle nanostructures is, certainly, at its infancy. The rapid advances in the area promise, however, a bright future to this scientific field. Interdisciplinary research efforts of chemists, biologists, physicists, and materials and computer scientists are anticipated to highlight the future perspectives of DNA nanotechnology.

AUTHOR INFORMATION

Corresponding Author

*E-mail: willnea@vms.huji.ac.il. Tel.: +972-2-56585272. Fax: +972-2-6527715.

BIOGRAPHIES

Ofer I. Wilner was born in 1978. He received his M.Sc. degree from the Tel-Aviv University in 2006 and performed his Ph.D. research at the Institute of Chemistry, The Hebrew University of Jerusalem (2006−2011). His research interests include DNA-based nanotechnology, biosensors, and artificial photosynthesis.

Itamar Willner completed his Ph.D. studies at The Hebrew University of Jerusalem in 1978. After postdoctoral research (1978−1981) at U.C. Berkeley, he joined the Institute of Chemistry at The Hebrew University of Jerusalem, where he was appointed as Professor in 1986. He coauthored over 600 research papers and monographs, and he serves on many editorial boards of journals. His research interests include bioelectronics and molecular electronics, nanobiotechnology, and, specifically, DNA-based nanotechnology, sensors and biosensors, application of metal and semiconductor nanoparticles for sensing, functional monolayer and thin film assemblies, light-induced electron-transfer processes and artificial photosynthesis, and supramolecular chemistry. He is the recipient of the Kolthoff Award, The Max-Planck Research Award for International Cooperation, the Israel Chemical Society Award (2001), the Israel Prize in Chemistry (2002), the Rothschild Prize (2008), and the EMET Prize (2008). He is a member of the Israel Academy of Sciences, the German National Academy of Sciences Leopoldina, and the European Academy of Sciences and Arts.

ACKNOWLEDGMENT

Our research on DNA nanotechnology is supported by the Israel Science Foundation and by the Volkswagen Foundation, Germany.

REFERENCES

(1) (a) Watson, J. D.; Crick, F. H. C. *Nature* **1953**, *171*, 737. (b) Sinden, R. R.; Pearson, C. E.; Potaman, V. N.; Ussery, D. W. *Adv. Gen. Biol.* **1998**, *5*, 1.

(2) Frank-Kamenetskii, M. D.; Mirkin, S. M. *Annu. Rev. Biochem.* **1995**, *64*, 65.

(3) Simonsson, T. *Biol. Chem.* **2001**, *382*, 621.

(4) Chen, L.; Cai, L.; Zhang, X.; Rich, A. *Biochemistry* **1994**, *33*, 13540.

(5) Miyake, Y.; Togashi, H.; Tashiro, M.; Yamaguchi, H.; Oda, S.; Kudo, M.; Tanaka, Y.; Kondo, Y.; Sawa, R.; Fujimoto, T.; Machinami, T.; Ono, A. *J. Am. Chem. Soc.* **2006**, *128*, 2172.

(6) Ritchie, C. M.; Johnsen, K. R.; Kiser, J. R.; Antoku, Y.; Dickson, R. M.; Petty, J. T. *J. Phys. Chem. C* **2007**, *111*, 175.

(7) Tanaka, K.; Clever, G. H.; Takezawa, Y.; Yamada, Y.; Kaul, C.; Shionoya, M.; Carell, T. *Nature Nanotechnol.* **2006**, *1*, 190.

(8) Goodchild, J. *Bioconjugate Chem.* **1990**, *1*, 165.

(9) (a) Nielsen, P. E.; Egholm, M.; Berg, R. H.; Buchardt, O. *Science* **1991**, *254*, 1497. (b) Egholm, M.; Buchardt, O.; Nielsen, P. E.; Berg, R. H. *J. Am. Chem. Soc.* **1992**, *114*, 1895. (c) Shakeel, S.; Karim, S.; Ali, A. *J. Chem. Technol. Biotechnol.* **2006**, *81*, 892.

(10) (a) Singh, S. K.; Koshkin, A. A.; Wengel, J.; Nielsen, P. *Chem. Commun.* **1998**, *4*, 455. (b) Kaur, H.; Arora, A.; Wengel, J.; Maiti, S. *Biochemistry* **2006**, *45*, 7347.

(11) (a) Bergmann, F.; Bannwarth, W.; Tam, S. *Tetrahedron Lett.* **1995**, *36*, 6823. (b) Kurreck, J.; Wyszko, E.; Gillen, C.; Erdmann, V. A. *Nucleic Acids Res.* **2002**, *30*, 1911.

(12) (a) Itakura, K.; Rossi, J. J.; Wallace, R. B. *Annu. Rev. Biochem.* **1984**, *53*, 323. (b) Lee, J. S.; Woodsworth, M. L.; Latimer, L. J. P.; Morgan, A. R. *Nucleic Acids Res.* **1984**, *12*, 6603. (c) Kool, E. T. *Chem. Rev.* **1997**, *97*, 1473.

(13) (a) Boon, E. M.; Ceres, D. M.; Drummond, T. G.; Hill, M. G.; Barton, J. K. *Nat. Biotechnol.* **2000**, *18*, 1096. (b) Drummond, T. G.; Hill, M. G.; Barton, J. K. *Nat. Biotechnol.* **2003**, *21*, 1192. (c) Drummond, T. G.; Hill, M. G.; Barton, J. K. *J. Am. Chem. Soc.* **2004**, *126*, 15010.

(14) (a) Evans, R. K.; Johnson, J. D.; Haley, B. E. *Proc. Natl. Acad. Sci. U. S. A.* **1986**, *83*, 5382. (b) Evans, R. K.; Haley, B. E. *Biochemistry* **1987**, *26*, 269. (c) Kielkopf, C. L.; Erkkila, K. E.; Hudson, B. P.; Barton, J. K.; Rees, D. C. *Nat. Struct. Biol.* **2000**, *7*, 117. (d) Liebmann, M.; Di Pasquale, F.; Marx, A. *ChemBioChem* **2006**, *7*, 1965.

(15) (a) Englisch, U.; Gauss, D. H. *Angew. Chem., Int. Ed.* **1991**, *30*, 613. (b) Nielsen, P. E. *J. Mol. Recognit.* **1990**, *3*, 1. (c) Ohndorf, U.-M.; Rould, M. A.; He, Q.; Pabo, C. O.; Lippard, S. J. *Nature* **1999**, *399*, 708. (d) Kelley, S. O.; Holmlin, R. E.; Stemp, E. D. A.; Barton, J. K. *J. Am. Chem. Soc.* **1997**, *119*, 9861. (e) Gierlich, J.; Burley, G. A.; Gramlich, P. M. E.; Hammond, D. M.; Carell, T. *Org. Lett.* **2006**, *8*, 3639.

(16) (a) Kornberg, A. *Trends Biochem. Sci.* **1984**, *9*, 122. (b) Zyskind, J. W.; Cleary, J. M.; Brusilow, W. S.; Harding, N. E.; Smith, D. W. *Proc. Natl. Acad. Sci. U. S. A.* **1983**, *80*, 1164. (c) Wefald, F. C.; Devlin, B. H.; Williams, R. S. *Nature* **1990**, *344*, 260. (d) Cusack, S. *Curr. Opin. Struct. Biol.* **1997**, *7*, 881.

(17) (a) Tuerk, C.; Gold, L. *Science* **1990**, *249*, 505. (b) Robertson, M. P.; Ellington, A. D. *Nat. Biotechnol.* **2001**, *19*, 650.

(18) (a) Stojanovic, M. N.; de Prada, P.; Landry, D. W. *J. Am. Chem. Soc.* **2001**, *123*, 4928. (b) Shlyahovsky, B.; Li, D.; Weizmann, Y.; Nowarski, R.; Kotler, M.; Willner, I. *J. Am. Chem. Soc.* **2007**, *129*, 3814. (c) Golub, E.; Pelossof, G.; Freeman, R.; Zhang, H.; Willner, I. *Anal. Chem.* **2009**, *81*, 9291. (d) Freeman, R.; Sharon, E.; Tel-Vered, R.; Willner, I. *J. Am. Chem. Soc.* **2009**, *131*, 5028.

(19) (a) Bock, L. C.; Griffin, L. C.; Latham, J. A.; Vermaas, E. H.; Toole, J. J. *Nature* **1992**, *355*, 564. (b) Macaya, R. F.; Schultze, P.; Smith, F. W.; Roe, J. A.; Feigon, J. *Proc. Natl. Acad. Sci. U. S. A.* **1993**, *90*, 3745. (c) Pavlov, V.; Xiao, Y.; Shlyahovsky, B.; Willner, I. *J. Am. Chem. Soc.* **2004**, *126*, 11768.

(20) (a) Cox, J. C.; Ellington, A. D. *Bioorg. Med. Chem.* **2001**, *9*, 2525. (b) Willner, I.; Zayats, M. *Angew. Chem., Int. Ed.* **2007**, *46*, 6408.

(21) (a) Breaker, R. R.; Joyce, G. F. *Chem. Biol.* **1994**, *1*, 223. (b) Joyce, G. F. *Annu. Rev. Biochem.* **2004**, *73*, 791. (c) Achenbach, J. C.; Chiuman, W.; Cruz, R. P. G; Li, Y. *Curr. Pharm. Biotechnol.* **2004**, *5*, 321. (d) Willner, I.; Shlyahovsky, B.; Zayats, M.; Willner, B. *Chem. Soc. Rev.* **2008**, *37*, 1153. (e) Sando, S.; Sasaki, T.; Kanatani, K.; Aoyama, Y. *J. Am. Chem. Soc.* **2003**, *125*, 15720.

(22) Hardin, C. C.; Corregan, M.; Brown, B. A., II; Frederick, L. N. *Biochemistry* **1993**, *32*, 5870.

(23) (a) Zhang, D. Y.; Winfree, E. *J. Am. Chem. Soc.* **2009**, *131*, 17303. (b) Seelig, G.; Soloveichik, D.; Zhang, D. Y.; Winfree, E. *Science* **2006**, *314*, 1585.

(24) (a) Tian, Y.; Mao, C. *J. Am. Chem. Soc.* **2004**, *126*, 11410. (b) Lin, C.; Liu, Y.; Yan, H. *Biochemistry* **2009**, *48*, 1663.

(25) (a) Yan, H.; Zhang, X.; Shen, Z.; Seeman, N. C. *Nature* **2002**, *415*, 62. (b) Benenson, Y.; Adar, R.; Paz-Elizur, T.; Livneh, Z.; Shapiro, E. *Proc. Natl. Acad. Sci. U. S. A.* **2003**, *100*, 2191. (c) Dittmer, W. U.; Reuter, A.; Simmel, F. C. *Angew. Chem., Int. Ed.* **2004**, *43*, 3550. (d) Beissenhirtz, M. K.; Willner, I. *Org. Biomol. Chem.* **2006**, *4*, 3392. (e) Bath, J.; Turberfield, A. J. *Nat. Biotechnol.* **2007**, *2*, 275.

(26) (a) Yurke, B.; Turberfield, A. J.; Mills, A. P., Jr.; Simmel, F. C.; Neumann, J. L. *Nature* **2000**, *406*, 605. (b) Niemeyer, C. M.; Adler, M. *Angew. Chem., Int. Ed.* **2002**, *41*, 3779. (c) Muller, B. K.; Reuter, A.; Simmel, F. C.; Lamb, D. C. *Nano Lett.* **2006**, *6*, 2814. (d) Elbaz, J.; Moshe, M.; Willner, I. *Angew. Chem., Int. Ed.* **2009**, *48*, 3834. (e) Elbaz, J.; Wang, Z.-G.; Orbach, R.; Willner, I. *Nano Lett.* **2009**, *9*, 4510.

(27) (a) Shin, J.-S.; Pierce, N. C. *J. Am. Chem. Soc.* **2004**, *126*, 10834. (b) Yin, P.; Yan, H.; Daniell, X. G.; Turberfield, A. J.; Reif, J. H. *Angew. Chem., Int. Ed.* **2004**, *43*, 4906. (c) Ding, B.; Seeman, N. C. *Science* **2006**, *314*, 1583. (d) Simmel, F. C. *ChemPhysChem* **2009**, *10*, 2593. (e) Omabegho, T.; Sha, R.; Seeman, N. C. *Science* **2009**, *324*, 67. (f) Wickham, S. F. J.; Endo, M.; Katsuda, Y.; Hidaka, K.; Bath, J.; Sugiyama, H.; Turberfield, A. J. *Nature Nanotechnol.* **2011**, *6*, 166.

(28) Wang, Z.-G.; Elbaz, J.; Willner, I. *Nano Lett.* **2011**, *11*, 304.

(29) Buranachai, C.; McKinney, S. A.; Ha, T. *Nano Lett.* **2006**, *6*, 496.

(30) (a) Tel-Vered, R.; Yehezkeli, O.; Yildiz, H. B.; Wilner, O. I.; Willner, I. *Angew. Chem., Int. Ed.* **2008**, *47*, 8272. (b) Piperberg, G.; Wilner, O. I.; Yehezkeli, O.; Tel-Vered, R.; Willner, I. *J. Am. Chem. Soc.* **2009**, *131*, 8724. (c) Elbaz, J.; Tel-Vered, R.; Freeman, R.; Yildiz, H. B.; Willner, I. *Angew. Chem., Int. Ed.* **2008**, *48*, 133. (d) Lund, K.; Manzo, A. J.; Dabby, N.; Michelotti, N.; Johnson-Buck, A.; Nangreave, J.; Taylor, S.; Pei, R.; Stojanovic, M. N.; Walter, N. G.; Winfree, E.; Yan, H. *Nature* **2010**, *465*, 206. (e) Gu, H.; Chao, J.; Xiao, S.-J.; Seeman, N. C. *Nature* **2010**, *465*, 202.

(31) (a) Weizmann, Y.; Beissenhirtz, M. K.; Cheglakov, Z.; Nowarski, R.; Kotler, M.; Willner, I. *Angew. Chem., Int. Ed.* **2006**, *45*, 7384. (b) Weizmann, Y.; Cheglakov, Z.; Willner, I. *J. Am. Chem. Soc.* **2008**, *130*, 17224. (c) Simmel, F. C. *Nanomedicine* **2007**, *2*, 817. (d) Moshe, M.; Elbaz, J.; Willner, I. *Nano Lett.* **2009**, *9*, 1196. (e) Teller, C.; Shimron, S.; Willner, I. *Anal. Chem.* **2009**, *81*, 9114. (f) Freeman, R.; Sharon, E.; Teller, C.; Willner, I. *Chem.—Eur. J.* **2010**, *16*, 3690.

(32) (a) Whitesides, G. M.; Mathias, J. P.; Seto, C. T. *Science* **1991**, *254*, 1312. (b) Lopinski, G. P.; Wayner, D. D. M.; Wolkow, R. A. *Nature* **2000**, *406*, 48. (c) Barth, J. V.; Costantini, G.; Kern, K. *Nature* **2005**, *437*, 671. (d) Gomar-Nadal, E.; Puigmarti-Luis, J.; Amabilino, D. B. *Chem. Soc. Rev.* **2008**, *37*, 490. (e) Li, D.; Wieckowska, A.; Willner, I. *Angew. Chem., Int. Ed.* **2008**, *47*, 3927. (f) Zhu, C.; Wen, Y.; Li, D.; Wang, L.; Song, S.; Fan, C.; Willner, I. *Chem.—Eur. J.* **2009**, *15*, 11898.

(33) (a) Lehn, J.-M. *Angew. Chem., Int. Ed.* **1988**, *27*, 89. (b) Stupp, S. I.; LeBonheur, V.; Walker, K.; Li, L. S.; Huggins, K. E.; Keser, M.; Amstutz, A. *Science* **1997**, *276*, 384. (c) Lehn, J.-M. *Science* **2002**, *295*, 2400. (d) Ikkala, O.; ten Brinke, G. *Science* **2002**, *295*, 2407. (e) Perham, R. N. *Philos. Trans. R. Soc., B* **1975**, *272*, 123.

(34) Ramakrishnan, V. *Cell* **2002**, *108*, 557.

(35) (a) Niemeyer, C. M. *Curr. Opin. Chem. Biol.* **2000**, *4*, 609. (b) Gothelf, K. V.; LaBean, T. H. *Org. Biomol. Chem.* **2005**, *3*, 4023. (c) Niemeyer, C. M.; Simon, U. *Eur. J. Inorg. Chem.* **2005**, *18*, 3641. (d) Lin, C.; Liu, Y.; Rinker, S.; Yan, H. *ChemPhysChem* **2006**, *7*, 1641. (e) LaBean, T. H.; Li, H. *Nano Today* **2007**, *2*, 26. (f) Niemeyer, C. M. *Angew. Chem., Int. Ed.* **2010**, *49*, 1200. (g) Simmel, F. C. *Angew. Chem., Int. Ed.* **2008**, *47*, 5884. (h) Aldaye, F. A.; Palmer, A. L.; Sleiman, H. F. *Science* **2008**, *321*, 1795. (i) Seeman, N. C. *Nano Lett.* **2010**, *10*, 1971.

(36) Liu, D.; Daubendiek, S. L.; Zillman, M. A.; Ryan, K.; Kool, E. T. *J. Am. Chem. Soc.* **1996**, *118*, 1587.
(37) Deng, Z.; Tian, Y.; Lee, S.-H.; Ribbe, A. E.; Mao, C. *Angew. Chem., Int. Ed.* **2005**, *44*, 3582.
(38) Zhao, W.; Gao, Y.; Kandadai, S. A.; Brook, M. A.; Li, Y. *Angew. Chem., Int. Ed.* **2006**, *45*, 2409.
(39) Beyer, S.; Nickels, P.; Simmel, F. C. *Nano Lett.* **2005**, *5*, 719.
(40) Hermann, T.; Patel, D. J. *Science* **2000**, *287*, 820.
(41) Cheglakov, Z.; Weizmann, Y.; Braunschweig, A. B.; Wilner, O. I.; Willner, I *Angew. Chem., Int. Ed.* **2007**, *47*, 126.
(42) Wilner, O. I.; Shimron, S.; Weizmann, Y.; Wang, Z.-G.; Willner, I. *Nano Lett.* **2009**, *9*, 2040.
(43) (a) Zayats, M.; Baron, R.; Popov, I.; Willner, I. *Nano Lett.* **2005**, *5*, 21. (b) Willner, I.; Baron, R.; Willner, B. *Adv. Mater.* **2006**, *18*, 1109. (c) Xiao, Y.; Pavlov, V.; Levine, S.; Niazov, T.; Markovitch, G.; Willner, I. *Angew. Chem., Int. Ed.* **2004**, *43*, 4519.
(44) (a) Baron, R.; Zayats, M.; Willner, I. *Anal. Chem.* **2005**, *77*, 1566. (b) Pavlov, V.; Xiao, Y.; Willner, I. *Nano Lett.* **2005**, *5*, 649.
(45) Basnar, B.; Weizmann, Y.; Cheglakov, Z.; Willner, I. *Adv. Mater.* **2006**, *18*, 713.
(46) (a) Mitra, D.; Di Cesare, N.; Sleiman, H. F. *Angew. Chem., Int. Ed.* **2004**, *43*, 5804. (b) Park, S. H.; Yin, P.; Liu, Y.; Reif, J. H.; LaBean, T. H.; Yan, H. *Nano Lett.* **2005**, *5*, 729.
(47) (a) Winfree, E.; Liu, F.; Wenzler, L. A.; Seeman, N. C. *Nature* **1998**, *394*, 539. (b) Mao, C.; Sun, W.; Seeman, N. C. *J. Am. Chem. Soc.* **1999**, *121*, 5437. (c) Chelyapov, N.; Brun, Y.; Gopalkrishnan, M.; Reishus, D.; Shaw, B.; Adleman, L. *J. Am. Chem. Soc.* **2004**, *126*, 13924. (d) Sharma, J.; Chhabra, R.; Liu, Y.; Ke, Y.; Yan, H. *Angew. Chem., Int. Ed.* **2006**, *45*, 730.
(48) (a) Chen, J.; Seeman, N. C. *Nature* **1991**, *350*, 631. (b) Mitchell, J. C.; Harris, J. R.; Malo, J.; Bath, J.; Turberfield, A. J. *J. Am. Chem. Soc.* **2004**, *126*, 16342. (c) Aldaye, F. A.; Sleiman, H. F. *J. Am. Chem. Soc.* **2007**, *129*, 4130.
(49) Fu, T. J.; Seeman, N. C. *Biochemistry* **1993**, *32*, 3211.
(50) LaBean, T. H.; Yan, H.; Kopatsch, J.; Liu, F.; Winfree, E.; Reif, J. H.; Seeman, N. C. *J. Am. Chem. Soc.* **2000**, *122*, 1848.
(51) Ke, Y.; Liu, Y.; Zhang, J.; Yan, H. *J. Am. Chem. Soc.* **2006**, *128*, 4414.
(52) Park, S. H.; Barish, R.; Li, H.; Reif, J. H.; Finkelstein, G.; Yan, H.; LaBean, T. H. *Nano Lett.* **2005**, *5*, 693.
(53) Mathieu, F.; Liao, S.; Kopatsch, J.; Wang, T.; Mao, C.; Seeman, N. C. *Nano Lett.* **2005**, *5*, 661.
(54) Petrillo, M. L.; Newton, C. J.; Chunningham, R. P.; Ma, R.-I.; Kallenbach, N. R.; Seeman, N. C. *Biopolymers* **1988**, *27*, 1337.
(55) Liu, D.; Wang, M.; Deng, Z.; Walulu, R.; Mao, C. *J. Am. Chem. Soc.* **2004**, *126*, 2324.
(56) Liu, Y.; Ke, Y.; Yan, H. *J. Am. Chem. Soc.* **2005**, *127*, 17140.
(57) Ding, B.; Sha, R.; Seeman, N. C. *J. Am. Chem. Soc.* **2004**, *126*, 10230.
(58) He, Y.; Chen, Y.; Liu, H.; Ribbe, A. E.; Mao, C. *J. Am. Chem. Soc.* **2005**, *127*, 12202.
(59) Xiao, S. J.; Liu, F. R.; Rosen, A. E.; Hainfeld, J. F.; Seeman, N. C.; Musier-Forsyth, K.; Kiehl, R. A. *J. Nanopart. Res.* **2002**, *4*, 313.
(60) Le, J. D.; Pinto, Y.; Seeman, N. C.; Musier-Forsyth, K.; Taton, T. A.; Kiehl, R. A. *Nano Lett.* **2004**, *4*, 2343.
(61) Zheng, J.; Constantinou, P. E.; Micheel, C.; Alivisatos, A. P.; Kiehl, R. A.; Seeman, N. C. *Nano Lett.* **2006**, *6*, 1502.
(62) Sharma, J.; Chhabra, R.; Cheng, A.; Brownell, J.; Liu, Y.; Yan, H. *Science* **2009**, *323*, 112.
(63) (a) Seeman, N. C.; Belcher, A. M. *Proc. Natl. Acad. Sci. U. S. A.* **2002**, *99*, 6451. (b) Endy, D. *Nature* **2005**, *438*, 449. (c) Heinemann, M.; Panke, S. *Bioinformatics* **2006**, *22*, 2790. (d) McDaniel, R.; Weiss, R. *Curr. Opin. Biotechnol.* **2005**, *16*, 476.
(64) He, Y.; Tian, Y.; Ribbe, A. E.; Mao, C. D. *J. Am. Chem. Soc.* **2006**, *128*, 15978.
(65) Yan, H.; Park, S. H.; Finkelstein, G.; Reif, J. H.; LaBean, T. H. *Science* **2003**, *301*, 1882.
(66) Ariyoshi, M.; Nishino, T.; Iwasaki, H.; Shinagawa, H.; Morikawa, K. *Proc. Natl. Acad. Sci. U. S. A.* **2000**, *97*, 8257.
(67) Malo, J.; Mitchell, J. C.; Venien-Bryan, C.; Harris, J. R.; Wille, H.; Sherratt, D. J.; Turberfield, A. J. *Angew. Chem., Int. Ed.* **2005**, *44*, 3057.
(68) (a) Selmi, D. N.; Adamson, R. J.; Attrill, H.; Goddard, A. D.; Gilbert, R. J.; Watts, A.; Turberfield, A. J. *Nano Lett.* **2011**, *11*, 657. (b) Goodman, R. P.; Erben, C. M.; Malo, J.; Ho, W. M.; McKee, M. L.; Kapanidis, A. N.; Turberfield, A. J. *ChemBioChem* **2009**, *10*, 1551.
(69) Liu, Y.; Lin, C.; Li, H.; Yan, H. *Angew. Chem., Int. Ed.* **2005**, *44*, 4333.
(70) Anderson, P. J. *Biochem. J.* **1998**, *336*, 631.
(71) Chhabra, R.; Sharma, J.; Ke, Y.; Liu, Y.; Rinker, S.; Lindsay, S.; Yan, H. *J. Am. Chem. Soc.* **2007**, *129*, 10304.
(72) Lin, C.; Katilius, E.; Liu, Y.; Zhang, J.; Yan, H. *Angew. Chem., Int. Ed.* **2006**, *45*, 5296.
(73) Cohen, J. D.; Sadowski, J. P.; Dervan, P. B. *Angew. Chem., Int. Ed.* **2007**, *46*, 7956.
(74) Cohen, J. D.; Sadowski, J. P.; Dervan, P. B. *J. Am. Chem. Soc.* **2008**, *130*, 402.
(75) Kuzuya, A.; Numajiri, K.; Komiyama, M. *Angew. Chem., Int. Ed.* **2008**, *47*, 3400.
(76) Rothemund, P. W. K. *Nature* **2006**, *440*, 297.
(77) (a) Jungmann, R.; Liedl, T.; Sobey, T. L.; Shih, W.; Simmel, F. C. *J. Am. Chem. Soc.* **2008**, *130*, 10062. (b) Ke, Y.; Sharma, J.; Liu, M.; Jahn, K.; Liu, Y.; Yan, H. *Nano Lett.* **2009**, *9*, 2445. (c) Douglas, S. M.; Dietz, H.; Liedl, T.; Hogberg, B.; Graf, F.; Shih, W. M. *Nature* **2009**, *459*, 414. (d) Dietz, H.; Douglas, S. M.; Shih, S. M. *Science* **2009**, *325*, 725. (e) Shih, W. M.; Lin, C. *Curr. Opin. Struct. Biol.* **2010**, *20*, 276. (f) Nangreave, J.; Han, D.; Liu, Y.; Yan, H. *Curr. Opin. Chem. Biol.* **2010**, *14*, 608.
(78) (a) www.cdna.dk/origami (accessed 2011). (b) http://cadnano.org/ (accessed 2011).
(79) Sharma, J.; Chhabra, R.; Andersen, C. S.; Gothelf, K. V.; Yan, H.; Liu, Y. *J. Am. Chem. Soc.* **2008**, *130*, 7820.
(80) Ding, B.; Deng, Z.; Yan, H.; Cabrini, S.; Zuckermann, R. N.; Bokor, J. *J. Am. Chem. Soc.* **2010**, *132*, 3248.
(81) (a) Kershner, R. J.; Bozano, L. D.; Micheel, C. M.; Hung, A. M.; Fornof, A. R.; Cha, J. N.; Rettner, C. T.; Bersani, M.; Frommer, J.; Rothemund, P. W. K.; Wallraff, G. M. *Nature Nanotechnol.* **2009**, *4*, 557. (b) Hung, A. M.; Micheel, C. M.; Bozano, L. D.; Osterbur, L. W.; Wallraff, G. M.; Cha, J. N. *Nature Nanotechnol.* **2010**, *5*, 121.
(82) Ding, B.; Wu, H.; Xu, W.; Zhao, Z.; Liu, Y.; Yu, H.; Yan, H. *Nano Lett.* **2010**, *10*, 5065.
(83) Lin, C.; Ke, Y.; Liu, Y.; Mertig, M.; Gu, J.; Yan, H. *Angew. Chem., Int. Ed.* **2007**, *46*, 6089.
(84) Gerdon, A. E.; Oh, S. S.; Hsieh, K.; Ke, Y.; Yan, H.; Soh, H. T. *Small* **2009**, *5*, 1942.
(85) Bui, H.; Onodera, C.; Kidwell, C.; Tan, Y.; Graugnard, E.; Kuang, W.; Lee, J.; Knowlton, W. B.; Yurke, B.; Hughes, W. L. *Nano Lett.* **2010**, *10*, 3367.
(86) Maune, H. T.; Han, S.-P.; Barish, R. D.; Bockrath, M.; Goddard, W. A., III; Rothemund, P. W. K.; Winfree, E. *Nature Nanotechnol.* **2010**, *5*, 61.
(87) (a) Rinker, S.; Ke, Y.; Liu, Y.; Chhabra, R.; Yan, H. *Nature Nanotechnol.* **2008**, *3*, 418. (b) Voigt, N. V.; Torring, T.; Rotaru, A.; Jacobsen, M. F.; Ravensbaek, J. B.; Subramani, R.; Mamdouh, W.; Kjems, J.; Mokhir, A.; Besenbacher, F.; Gothelf, K. V. *Nature Nanotechnol.* **2010**, *5*, 200.
(88) Sacca, B.; Meyer, R.; Erkelenz, M.; Kiko, K.; Arndt, A.; Schroeder, H.; Rabe, K. S.; Niemeyer, C. M. *Angew. Chem., Int. Ed.* **2010**, *49*, 9378.
(89) Los, G. V.; Wood, K. *Methods Mol. Biol.* **2007**, *356*, 195.
(90) Regoes, A.; Hehl, A. B. *BioTechniques* **2005**, *39*, 809.
(91) Kuzuya, A.; Kimura, M.; Numajiri, K.; Koshi, N.; Ohnishi, T.; Okada, F.; Komiyama, M. *ChemBioChem* 2009, *10*, 1811.
(92) Numajiri, K.; Kimura, M.; Kuzuya, A.; Komiyama, M. *Chem. Commun.* **2010**, *46*, 5127.
(93) Andersen, E. S.; Dong, M.; Nielsen, M. M.; Jahn, K.; Subramani, R.; Mamdouh, W.; Golas, M. M.; Sander, B.; Stark, H.; Oliveira, C. L. P.;

Pedersen, J. S.; Birkedal, V.; Besenbacher, F.; Gothelf, K. V.; Kjems, J. *Nature* **2009**, *459*, 73.
(94) Mastroianni, A. J.; Claridge, S. A.; Alivisatos, A. P. *J. Am. Chem. Soc.* **2009**, *131*, 8455.
(95) Aldaye, F. A.; Sleiman, H. F. *J. Am. Chem. Soc.* **2007**, *129*, 4130.
(96) (a) Lazarides, A. A.; Schatz, G. C. *J. Phys. Chem. B* **2000**, *104*, 460. (b) Mirkin, C. A.; Letsinger, R. L.; Mucic, R. C.; Storhoff, J. J. *Nature* **1996**, *382*, 607. (c) Nam, J.-M.; Park, S.-J.; Mirkin, C. A. *J. Am. Chem. Soc.* **2002**, *124*, 3820.
(97) (a) Park, S. Y.; Lytton-Jean, A. K. R.; Lee, B.; Weigand, S.; Schatz, G. C.; Mirkin, C. A. *Nature* **2008**, *451*, 553. (b) Nykypanchuk, D.; Maye, M. M.; van der Lelie, D.; Gang, O. *Nature* **2008**, *451*, 549.
(98) Lo, P. K.; Karam, P.; Aldaye, F. A.; McLaughlin, C. K.; Hamblin, G. D.; Cosa, G.; Sleiman, H. F. *Nature Chem.* **2010**, *2*, 319.
(99) Weizmann., Y.; Braunschweig, A. B.; Wilner, O. I.; Cheglakov, Z.; Willner, I. *Chem. Commun.* **2008**, *40*, 4888.
(100) (a) Wilson, D. S.; Szostak, J. W. *Annu. Rev. Biochem.* **1999**, *68*, 611. (b) Famulok, M.; Mayer, G.; Blind, M. *Acc. Chem. Res.* **2000**, *33*, 591.
(101) Stojanovic, M. N.; de Prada, P.; Landry, D. W. *J. Am. Chem. Soc.* **2000**, *122*, 11547.
(102) (a) Jayasena, S. D. *Clin. Chem.* **1999**, *45*, 1628. (b) Liu, J.; Lu, Y. *Angew. Chem., Int. Ed.* **2006**, *45*, 90. (c) Tombelli, S.; Minunni, M.; Mascini, M. *Biosens. Bioelectron.* **2005**, *20*, 2424. (d) Yoshida, W.; Sode, K.; Ikebukuro, K. *Anal. Chem.* **2006**, *78*, 3296. (e) Freeman, R.; Sharon, E.; Tel-Vered, R.; Willner, I. *J. Am. Chem. Soc.* **2009**, *131*, 5028. (f) Freeman, R.; Li, Y.; Tel-Vered, R.; Sharon, E.; Elbaz, J.; Willner, I. *Analyst* **2009**, *134*, 653. (g) Baker, B. R.; Lai, R. Y.; Wood, M. S.; Doctor, E. H.; Heeger, A. J.; Plaxco, K. W. *J. Am. Chem. Soc.* **2006**, *128*, 3138. (h) Gronewold, T. M. A.; Glass, S.; Quandt, E.; Famulok, M. *Biosens. Bioelectron.* **2005**, *20*, 2044. (i) Famulok, M.; Hartig, J. S.; Mayer, G. *Chem. Rev.* **2007**, *107*, 3715.
(103) Wang, Z.-G.; Wilner, O. I.; Willner, I. *Nano Lett.* **2009**, *9*, 4098.
(104) Weizmann, Y.; Braunschweig, A. B.; Wilner, O. I.; Cheglakov, Z.; Willner, I. *Proc. Natl. Acad. Sci. U. S. A.* **2008**, *105*, 5289.
(105) Wilner, O. I.; Weizmann, Y.; Gill, R.; Lioubashevski, O.; Freeman, R.; Willner, I. *Nature Nanotechnol.* **2009**, *4*, 249.
(106) Reches, M.; Gazit, E. *Science* **2003**, *300*, 625.
(107) Braun, E.; Eichen, Y.; Sivan, U.; Ben-Yoseph, G. *Nature* **1998**, *391*, 775.
(108) Keren, K.; Berman, R. S.; Buchstab, E.; Sivan, U.; Braun, E. *Science* **2003**, *302*, 1380.
(109) (a) Miller, R. V.; Kokjohn, T. A. *Annu. Rev. Microbiol.* **1990**, *44*, 365. (b) Lusetti, S. L.; Cox, M. M. *Annu. Rev. Biochem.* **2002**, *71*, 71.
(110) Nishinaka, T.; Takano, A.; Doi, Y.; Hashimoto, M.; Nakamura, A.; Matsushita, Y.; Kumaki, J.; Yashima, E. *J. Am. Chem. Soc.* **2005**, *127*, 8120.
(111) Richter, J.; Mertig, M.; Pompe, W.; Monch, I.; Schackert, H. K. *Appl. Phys. Lett.* **2001**, *78*, 536.
(112) Dong, L.; Hollis, T.; Connolly, B. A.; Wright, N. G.; Horrocks, B. R.; Houlton, A. *Adv. Mater.* **2007**, *19*, 1748.
(113) Park, S. H.; Barish, R.; Li, H.; Reif, J. H.; Finkelstein, G.; Yan, H.; LaBean, T. H. *Nano Lett.* **2005**, *5*, 693.
(114) Liu, D.; Park, S. H.; Reif, J. H.; LaBean, T. H. *Proc. Natl. Acad. Sci. U. S. A.* **2004**, *101*, 717.
(115) Patolsky, F.; Weizmann, Y.; Willner, I. *Nature Mater.* **2004**, *3*, 692.